

**SYNTHESIS OF NOVEL COLLOIDAL BUILDING
BLOCKS FOR DIRECTED SELF-ASSEMBLY**

By

JIAN XU

Bachelor of Engineering

Central South University

Changsha, P.R. China

1998


Submitted to the Faculty of the
Graduate College of the
Oklahoma State University
in partial fulfillment of
the requirements for
the Degree of
MASTER OF SCIENCE
December, 2004

**SYNTHESIS OF NOVEL COLLOIDAL BUILDING
BLOCKS FOR DIRECTED SELF-ASSEMBLY**

Thesis Approved:



Thesis Advisor



Warren T Ford



Dean of the Graduate College

To my parents

Xu, Jinlin and Hu, Ping

ACKNOWLEDGEMENTS

First of all, I owe my deepest gratitude to my parents, Xu, Jinlin, and Hu, Ping. They endowed all the nourishment and encouragement to bring me up a man with integrity, and supported me financially to their best to make my studying at OSU possible. All my achievements so far are inseparable part of theirs.

Second, I would like to give my sincere appreciation to the dedicated faculty and staff in School of Chemical Engineering, especially my advisor Dr. James E. Smay. He provides me a comfortable environment to explore my creativity and scientific curiosity under his intelligent guidance. Special appreciation also goes to Dr. Robert L. Robinson Jr. and Dr. Khaled A.M. Gasem for the trust and support I received from them.

Acknowledgements also go to Dr. Weili Zhang in School of Electrical and Computer Engineering and Dr. Warren T. Ford in Department of Chemistry. Without their guidance and contribution of time, this work could not have gone this far.

I would like to thank my colleagues and friends Baojun Xie, Sarosh Nadkarni, Yuguang Zhao, Xiaoming Jiang, and all those who had helped me since I came to Stillwater. They have made it an invaluable experience to study at OSU.

TABLE OF CONTENTS

Chapter	Page
1. OBJECTIVES.....	1
1.1 Background.....	1
1.2 Thesis Objectives.....	9
1.3 Thesis Organization.....	10
References.....	12
2. SYNTHESIS OF MONODISPERSE POLYMER MICROSPHERES.....	16
2.1 Introduction.....	16
2.2 Experimental.....	19
2.2.1 Materials.....	19
2.2.2 Instrumentation.....	19
2.2.3 Particle Synthesis.....	20
2.2.4 Separation and Filtration.....	22
2.3 Results and discussion.....	23
References.....	32
3. SURFACE MODIFICATION OF POLYSTYRENE MICROSPHERES.....	34
3.1 Introduction.....	34
3.2 Experimental	38
3.2.1 Materials.....	38
3.2.2 Synthesis of Boc-p-Aminostyrene Comonomer.....	39
3.2.3 Two-Stage Dispersion Polymerization.....	40
3.2.4 Acidic Cleavage.....	42
3.2.5 Synthesis of Au Nanoparticles.....	42
3.2.6 Stabilizer Exchange on Polystyrene and Aminated Polystyrene Particles.....	44
3.2.7 Adsorption of Au Nanoparticles on Aminated Polystyrene Particles.....	45
3.2.8 Gold Nanoshell Growth.....	46
3.3 Results and discussion.....	46
3.3.1 Amine Functionalization of Polystyrene Particles.....	46
3.3.2 Stabilizer Removal and Exchange.....	49
3.3.3 Gold Nanoparticle Adsorption and	

Gold Nanoshell Assembly.....	50
References.....	59
4. FABRICATION OF COLLOIDAL BUILDING BLOCKS.....	61
4.1 Introduction.....	61
4.2 Experimental.....	67
4.2.1 Materials.....	67
4.2.2 Instrumentation.....	67
4.2.3 Photomask Fabrication.....	68
4.2.4 Photolithography.....	72
4.2.5 Modified TASA Method.....	74
4.3 Results and Discussion.....	78
4.3.1 Photomask Fabrication.....	78
4.3.2 Photolithography.....	78
4.3.3 Modified TASA Method.....	82
References.....	88
5. CONCLUSIONS AND RECOMMENDATIONS.....	90
5.1 Conclusions.....	90
5.2 Recommendations and Future Work.....	93
5.2.1 Process Optimization.....	94
5.2.2 Recommended Future Work.....	95

LIST OF TABLES

Table	Page
2.1 Particle size under different reaction conditions.....	27
2.2 Statistical calculations of sizes of the monodisperse polystyrene microspheres.....	27
4.1 Dimensions of the patterns in column 1 and column 2 in the mask design (μm).....	71
4.2 Dimensions of the patterns in column 3 and column 4 in the mask design (μm).....	71

LIST OF FIGURES

Figure		Page
1.1	One-dimensional and two-dimensional photonic crystals (a) multi-layered films, (b) square lattice of dielectric columns.....	2
1.2	Three-dimensional photonic crystals through different methods (a) Lincoln-log structure through MEMS, (b) true diamond lattice through micro-manipulation, (c) photonic crystal structure fabricated through holographic lithography, (d) inverse opal through chemical vapor deposition (CVD).....	3
1.3	FCC (100) lattice in grooved silicon template, (b) FCC (100) lattice on pyramidal pits, (c) silica colloidal crystal films produced by IHEISA method, (d) porous metallic gold structure.....	6
1.4	TASA process (a) photolithography to fabricate patterned arrays of templates on a substrate, (b) an aqueous dispersion of spherical colloids confined within the fluidic cell was allowed to dewet across the cell, (c) capillary force pushing the spheres across the surface of the template on the substrate and the physically trapped particles.....	7
1.5	SEM images of colloidal aggregates that were assembled through TASA strategy (a) triangular aggregates composed of silica and PS spheres, (b) square aggregates composed of PS beads, (c) tetrahedrons composed of PS beads in cylindrical holes, (d) ring-shaped aggregates composed of PS beads.....	8
1.6	A schematic illustration of the building block to be assembled, consisting of one central PS microsphere and two functionalized PS microspheres at satellite positions; particles are annealed together through thermal treatment above the glass transition temperature.....	9

2.1	Free radical polymerization of styrene as in suspension, emulsion and dispersion polymerization.....	18
2.2	Dispersion polymerization apparatus: (1) reflux condenser, (2) 3-necked distilling flask with nitrogen blanket, (3) mineral oil bath with magnetic stirring and heating coil, (4) hot plate.....	21
2.3	Polystyrene particles synthesized through dispersion polymerization (a) SEM image of sputter-coated 6.4 μm polystyrene microspheres, (b) SEM image of sputter-coated 6.4 μm polystyrene particles with large outliers, (c) optical image of 6.4 μm polystyrene microspheres.....	25
2.4	SEM images of sputter-coated polystyrene particles synthesized at different ethanol/1-methoxy-2-propanol ratios, where 15 mL styrene monomer, 2 g HPC and 1g BPO were used (a) 60 mL / 25 mL, (b) 50 mL / 35 mL, (c) 47.5 mL / 37.5 mL, (d) 45 mL/ 40 mL, (e) 42.5 mL / 42.5 mL, (f) 40 mL / 45 mL.....	26
2.5	SEM images of sputter-coated polystyrene particles synthesized with different stabilizer concentrations, where 15 mL styrene monomer, 47.5 mL ethanol, 37.5 mL 1-methoxy-2-propanol and 1g BPO were used, (a) 1.5 g HPC, (b) 1.25 g HPC, (c) 1 g HPC.....	29
2.6	SEM images of sputter-coated polystyrene particles synthesized with different initiator concentrations, where 15 mL styrene monomer, 47.5 mL ethanol, 37.5 mL 1-methoxy-2-propanol and 2 g HPC were used (a) 0.75 g BPO, (b) 0.5 g BPO.....	30
3.1	Schematic illustration of a triplet building block to be self-assembled: A—the polystyrene microspheres at the center, B—the amine-functionalized particles with gold nanoshells, C—the thiolized oligonucleotides attached to the Au particles through the gold-thiol binding.....	36
3.2	Schematic illustration of the two-stage dispersion polymerization technique: A—formation of polystyrene microspheres from precipitated polymer chains, B—size growth of the substrate polystyrene microspheres, C—formation of a copolymeric layer on the surface of existing polystyrene substrate.....	38

3.3	Protection of amine group on 4-aminostyrene using di-tert-butyl dicarbonate.....	40
3.4	The copolymerization of the styrene monomer and the Boc-p-aminostyrene monomer.....	41
3.5	Generation of the ionized amine groups on the polystyrene/Boc-p-aminostyrene copolymeric particles through acidic cleavage.....	42
3.6	FTIR spectra for (a) Boc-p-aminostyrene monomer, (b) functionalized polystyrene/Boc-p-aminostyrene, and (c) amine functionalized polystyrene particles.....	49
3.7	Flocculated polystyrene particles in ethanol, when the HPC stabilizer molecules were not available.....	50
3.8	Effectively positively charged HPC molecules attached to the surface of a polystyrene particle in acidic solution.....	51
3.9	SEM images of Au nanoparticles coated HPC stabilized polystyrene particles.....	52
3.10	Adsorption test (a) white sediment after mixing Au nanoparticles with F108 stabilized plain polystyrene particles; (b) reddish sediment after mixing Au nanoparticles with HPC stabilized plain polystyrene particles.....	54
3.11	SEM images showing Au-polystyrene composite particles with (a) Au nanoparticles from sodium citrate reduction (b) Au nanoparticles from THPC reduction.....	55
3.12	SEM images of Au nanoshell composite particles (a) 3.8 μm sized Au nanoshell composite particles (b) the surface of a Au nanoshell composite particle.....	57
4.1	A dewetting fluidic cell for trapping spherical particles.....	62
4.2	Illustration of a general photolithography process.....	64
4.3	Principles of lithography illustrated for positive and negative resists.....	65
4.4	A relief photoresist structure trapping two 4 μm polystyrene particles atop one 6.4 μm polystyrene	

particles (a) perspective view (b) cross section view with dimensions.....	69
4.5 Layout of the array of the pattern sets on the photomask for the negative photoresist.....	70
4.6 Shape of patterns in column 1 and column 2 on the mask design, consisting of 3 circles.....	70
4.7 Shape of patterns in column 3 and column 4 on the mask design, consisting of two small circles and one big ellipse.....	71
4.8 Kasper Wafer Alignment Systems, Kasper 2001	72
4.9 Monodisperse polystyrene microspheres synthesized for the second step trapping.....	77
4.10 Schematic illustration of isotropic and anisotropic etching occurred during photoresist development.....	79
4.11 A template fabricated with the photomask and the negative photoresist.....	80
4.12 A positive template for trapping monodisperse 4.0 μm polystyrene particles.....	81
4.13 6.4 μm polystyrene microspheres trapped (a) at the center of the template holes in region C-4, (b) when the template holes (in region D-1) were with poor geometries; two particles were trapped in a single hole.....	81
4.14 Triplet aggregates trapped in the template holes.....	82
4.15 particles of 4 μm diameter trapped in 4.7 μm holes; with some vacant holes.....	83
5.1 (a) A tetrahedral building block (to be assembled) without the template; (b) a tetrahedral building block structure trapped in the template (solid); (c) a tetrahedral building block structure trapped in the template (transparent); (d) a diamond-like lattice to be assembled from the tetrahedral building blocks.....	96
5.2 The illustration of a possible template strategy for assembling the tetrahedral shaped colloidal building	

blocks (a) the particles trapped in the first layer, (b) the tetrahedral building block structure assembled after the second layer trapping, (c) a side view of the template and the building block assembled, (d) dissolving the top template to release the building block.....	97
---	----

NOMENCLATURE

2D	two-dimensional
3D	three-dimensional
BPO	benzoyl peroxide
CBB	colloidal building block
CMP	chemical mechanical planarization
CVD	chemical vapor deposition
DI	deionized
FCC	face-centered cubic
FFF	field flow fractionation
HCl	hydrochloric acid
HCP	hexagonal closest packing
HPC	hydroxypropyl cellulose
IHEISA	isothermal heating evaporation induced self-assembly
IPA	isopropyl alcohol/2-propanol/isopropanol
MEMS	Micro-Electro-Mechanical Systems
MW	molecular weight
PBG	photonic band gap
PEI	polyethylenimine
rcf	relative centrifugal force

RIE	reactive ion etching
SDS	sodium dodecyl sulfate
TASA	template-assisted self-assembly
T_g	glass transition temperature
THPC	tetrakis(hydroxymethyl)phosphonium chloride
UV	ultraviolet

Chapter 1

OBJECTIVES

1.1 Background

A photonic crystal is a periodic dielectric structure that forbids the propagation of electromagnetic waves within a certain frequency spectrum, known as the photonic band gap (PBG). The origin of the PBG lies in the periodic variation of the low loss dielectric structure that gives rise to scattering and destructive interference, resulting in near zero density of states for propagation¹. Photonic crystals of this kind are also called PBG materials.

A one-dimensional photonic crystal structure consists of alternating layers of materials with high contrast dielectric constants, commonly known as a dielectric mirror, Figure 1.1a; two-dimensional, Figure 1.1b, and three-dimensional photonic crystals extend symmetry and periodicity along two and three axes respectively. One may predict the PBG by solving the Maxwell Equations in the context of the periodic dielectrics²⁻⁴.

The PBG may be exploited to enable light manipulation that is impossible to achieve with conventional optics. Resonant cavities may be created within the PBG crystal when point defects are introduced into the structure, where light modes within the band gap can be localized. Many applications, such as channel-drop filters⁵, sharp bend waveguides⁶, waveguide crossings⁷, and wide-angle splitters⁸, have been proposed. The

main advantage of using PBG materials is lower energy loss and device miniaturization that is impossible using optical fibers and mirrors.

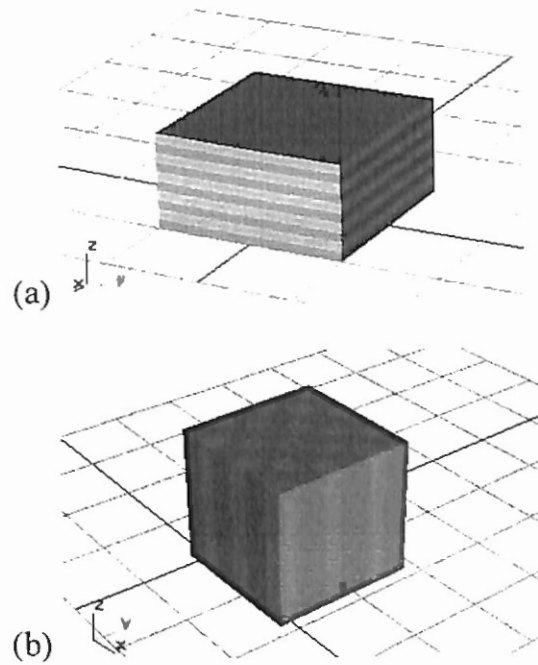


Figure 1.1 One-dimensional and two-dimensional photonic crystals (a) multi-layered films, (b) square lattice of dielectric columns

Though conceptually simple, photonic crystals have been difficult to fabricate in that the required periodicity should be comparable to the wavelengths of light and the symmetry of the structure must be carefully controlled. To date, a variety of fabrication strategies have been developed, such as glancing angle deposition⁹, Micro-Electro-Mechanical Systems (MEMS) technology¹⁰⁻¹⁶, Figure 1.2a, micro-manipulation¹⁷, Figure 1.2b, layer-by-layer lithography¹⁸, holographic lithography¹⁹, Figure 1.2c, self-assembly of colloidal particles²⁰, synthetic block copolymer method²¹ and “Yablonovite” method²². Among these, holographic lithography, MEMS and self-assembly strategies are the most promising ones for fabrication and commercialization of PBG materials.

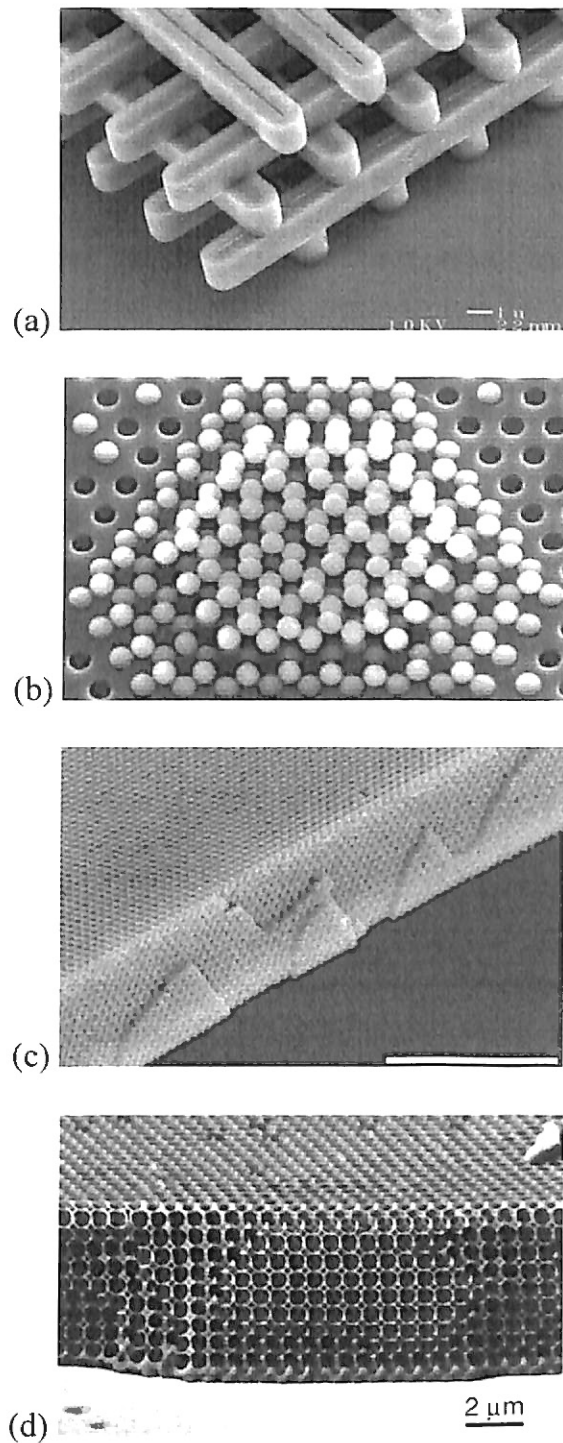


Figure 1.2 Three-dimensional photonic crystals through different methods (a) Lincoln-log structure through MEMS¹⁰, (b) true diamond lattice through micro-manipulation¹⁷, (c) photonic crystal structure fabricated through holographic lithography¹⁹, (d) inverse opal through chemical vapor deposition (CVD)²³

Based upon fundamentals of light interference, holographic lithography utilizes four coherent laser beams so that defect-free and high-resolution three-dimensional photonic crystal structures over large areas can be created out of a photoresist layer, Figure 1.2c. By choosing the appropriate direction, intensity and polarization relationships among the laser beams, the structures of the resulting interference pattern can be manipulated. Holographic lithography demands extreme precision, which is largely focused on the quality of the point source and laser beam delivery. Furthermore, suitable high-refractive-index filler needs to be imbibed into the structure to achieve the required dielectric contrast.

MEMS technology involves using well-developed processes such as CVD, chemical mechanical planarization (CMP), photolithography, reactive ion etching (RIE) and surface micromachining to manufacture micron-sized structures. Through MEMS technology, photonic crystals, Figure 1.2a, have been effectively fabricated with materials such as silicon and tungsten¹⁰⁻¹⁶, which are explored as high-efficiency light source and optical switches. MEMS technology requires tremendous investment in setting up processing lines. The achievable feature size of the PBG structure is ordinarily within micron-size range, which limits the PBG that can be devised.

Employed mainly for nano-scale and micro-scale fabrication, the self-assembly strategy involves designing building-block entities that aggregate in a controllable manner to yield periodic lattice structures. The self-assembly strategy carries out steps using highly developed synthetic chemistry, frequently draws inspiration from examples in biology and sometimes incorporates biological entities. Examples of self-assembly, not necessarily for PBG application, are the creation of polymers^{24,25}, proteins²⁶, and

molecular assemblies²⁷, and the fabrication of structures consisting of patterned meso-scale objects²⁸ or tiny robots²⁹.

The self-assembly of readily synthesized colloidal spheres appears to be a cost effective method to fabricate PBG crystals of bulk dimensions. Initial efforts have been focused on sedimentation of monodisperse and bimodal particles, Figure 1.3a, into stable crystal structure. More recently, patterned substrates, Figure 1.3b and 1.3c, have been used to template the first layer of the colloidal crystals to improve long-range quality and impose some control over crystal orientation²⁰. These strategies are a macroscopic analog to the natural assembly of metallic crystals with spherical bonding symmetry. They lack the selective directional bonding associated with covalently bonded crystals. As with metals and alloys, point and line defects in simple colloidal crystals are numerous. Additionally, controlling the location of defects within the crystal is extremely difficult. Often, an inverse structure, Figure 1.3d, achieved through infiltration of high refractive index materials, e.g. silicon, Figure 1.2d, into the interstitial void space in a pre-assembled photonic crystals is needed²³. Most recently, limited work to synthesize and self-assemble non-spherical building blocks³⁹⁻⁴⁵ has been explored.

Younan Xia and coworkers have demonstrated the template-assisted self-assembly (TASA)⁴⁶ strategy which combines physical confinement and capillary forces to assemble monodisperse spherical colloids into uniform aggregates with well-controlled sizes, shapes, and structures. Patterned arrays of templates on a substrate were produced using photolithography, Figure 1.4a, from which a fluidic cell was fabricated. Subsequently, an aqueous dispersion of spherical colloids that had been confined within

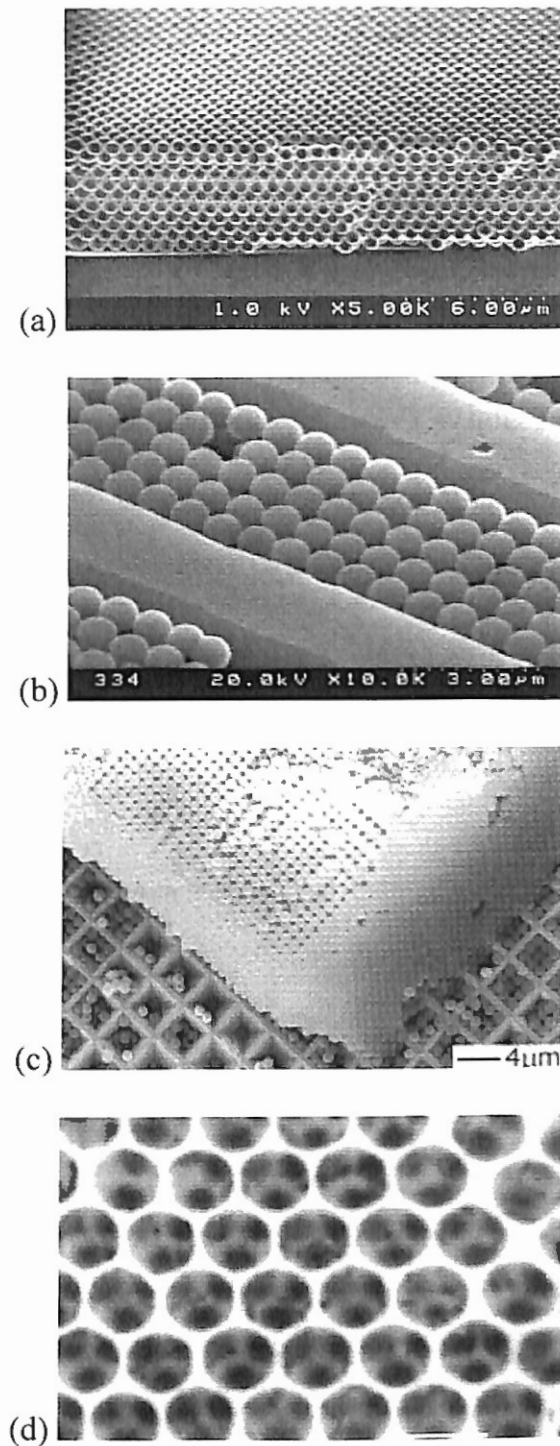


Figure 1.3 (a) FCC (100) lattice in grooved silicon template⁴⁷, (b) FCC (100) lattice on pyramidal pits²⁰, (c) silica colloidal crystal films produced by IHEISA method³², (d) porous metallic gold structure⁴⁸

the fluidic cell was allowed to dewet slowly across the cell, Figure 1.4b. The capillary force exerted on the rear edge of this liquid slug would push the spheres across the surface of the template on the substrate until the particles were physically trapped, Figure 1.4c. The resulting aggregates can be released through sonication or dissolving the template, if possible. The aggregates thereby formed, Figure 1.5, could be used as building blocks for the assembly of photonic crystals. While TASA is a clever way to alter the building block structure, the bonding in the colloidal crystal is still analogous to that of metals. The capability of TASA to define the 3D structure of the building blocks, and to allow for differentiation of the chemistry within a single building block has yet to be fully exploited.

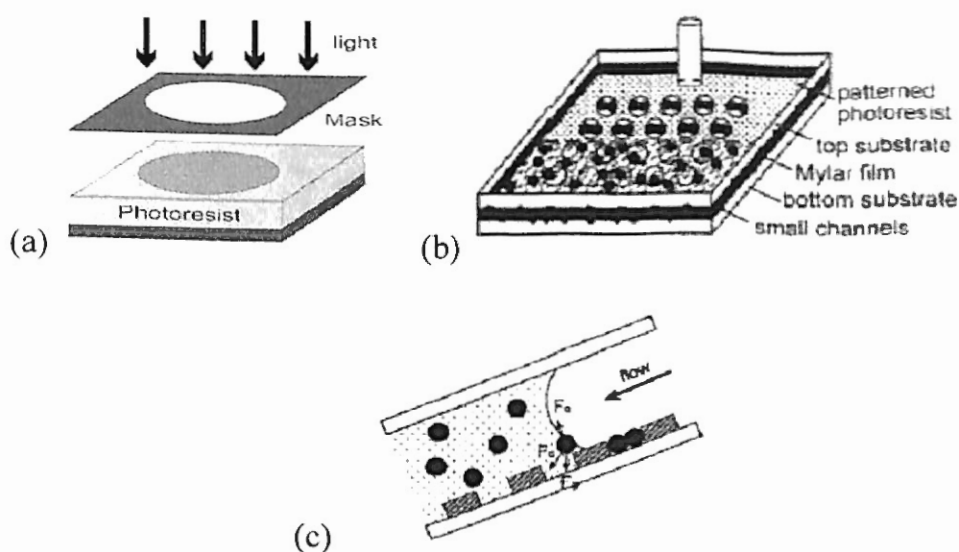


Figure 1.4 TASA process (a) photolithography to fabricate patterned arrays of templates on a substrate, (b) an aqueous dispersion of spherical colloids confined within the fluidic cell was allowed to dewet across the cell, (c) capillary force pushing the spheres across the surface of the template on the substrate and the physically trapped particles

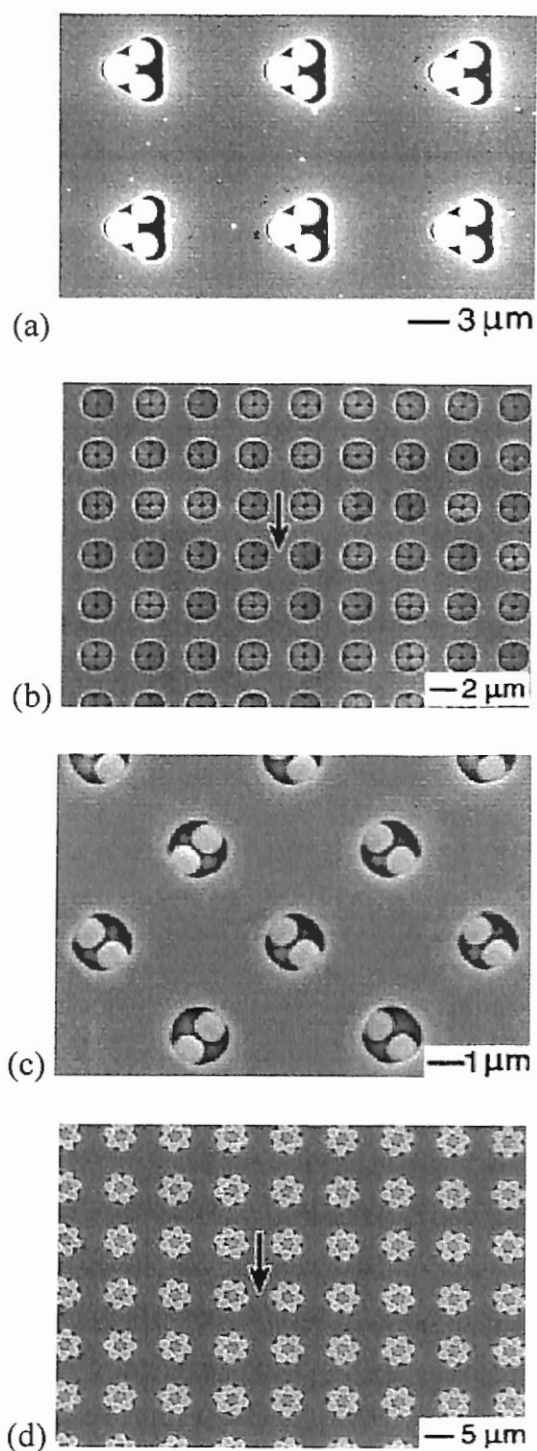


Figure 1.5 SEM images of colloidal aggregates that were assembled through TASA strategy (a) triangular aggregates composed of silica and PS spheres, (b) square aggregates composed of PS beads, (c) tetrahedrons composed of PS beads in cylindrical holes, (d) ring-shaped aggregates composed of PS beads⁴⁶

1.2 Thesis Objectives

Theoretical studies have indicated that monodisperse spherical particles are not well suited as the building blocks in generating photonic crystals with complete band gaps due to degeneracy in the photonic band structure caused by the spherical symmetry of the lattice points. In this regard, non-spherical particles will offer some immediate advantages over their spherical counterparts in applications that require lattices with lower symmetries and higher complexities.

The overarching objective of this work is to create colloidal building blocks with controlled structure and surface chemistry, Figure 1.6, to introduce geometric as well as selective, directional bonding to the self-assembly process.

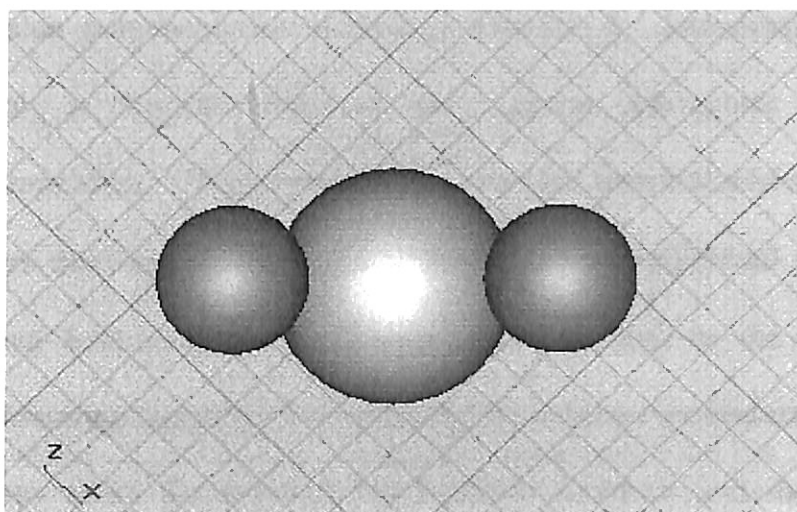


Figure 1.6 A schematic illustration of the building block to be assembled, consisting of one central PS microsphere and two functionalized PS microspheres at satellite positions: particles are annealed together through thermal treatment above the glass transition temperature (T_g).

Two types of monodisperse microspheres with difference size ranges and surface chemistries are to be synthesized. Traditional photolithography is to be explored to generate templates for the modified TASA process. Geometrically complex designer building blocks are to be fabricated through trapping those synthesized microspheres with templates in a fluidic cell. Fabricated building blocks can be released from the templates through sonication. Preliminary study on the self-assembly of colloidal crystal lattice by tuning the geometric structures and surface chemistries of the fabricated building blocks is the next step in future work.

1.3 Thesis Organization

In chapter two, synthesis of monodisperse polystyrene microspheres using a modified dispersion polymerization method is introduced. Introduction of functional groups, preferably in the outer layer of monodisperse polystyrene microspheres, is described in chapter three. Chapter four investigates the template-assisted self-assembly strategy. Factors that lead to the successful trapping of individual particles and the formation of final hetero-structured building blocks as well as the photolithography technique for fabricating templates for self-assembly process are discussed. Chapter five draws conclusions about the polymer microsphere synthesis and the building block assembly process. Finally, important concepts and future directions such as geometric versatility of the building blocks, sequential trapping with multi-layered templates, field-assisted self-assembly^{37,50-52}, selectivity⁴⁹ and directionality of inter-particulate functional interactions, and designability of resulting colloidal crystal lattice, which endow great

possibility and flexibility to the self-assembly process, however overlooked or segregated in many contemporary works, are to be discussed in chapter six.

References

1. J. D. Joannopoulos, R. D. Meade and J. N. Winn, *Photonic crystals: molding the flow of light*, 1995.
2. A. Reineix and B. Jecko, *Annales Des Telecommunications-Annals of Telecommunications*, **51**, 656-662 (1996).
3. M. Thevenot, A. Reineix and B. Jecko, *Journal of Optics a-Pure and Applied Optics*, **1**, 495-500 (1999).
4. M. Thevenot, A. Reineix and B. Jecko, *Microwave and Optical Technology Letters*, **21**, 25-28 (1999).
5. S. Fan, P. R. Villeneuve and J. D. Joannopoulos, *Physical Review Letters*, **80**, 960-963 (1998).
6. A. Mekis, J. C. Chen, I. Kurland, S. Fan, P. R. Villeneuve and J. D. Joannopoulos, *Physical Review Letters*, **77**, 3787-3790 (1996).
7. S. G. Johnson, C. Manolatou, S. Fan, R. Villeneuve, J. D. Joannopoulos and H. A. Haus, *Optics Letters*, **23**, 1855 (1998).
8. S. Fan, S. G. Johnson, J. D. Joannopoulos, C. Manolatou and H. A. Haus, *Journal of Optical Society of America B*, **18**, 162 (2001).
9. O. Toader and S. John, *Science*, **292**, 1133-1135 (2001).
10. S. Y. Lin, J. G. Fleming, D. L. Hetherington, B. K. Smith, R. Biswas, K. M. Ho, M. M. Sigalas, W. Zubrzycki, S. R. Kurtz and J. Bur, *Nature*, **394**, 251 - 253 (1998).
11. S. Y. Lin, J. G. Fleming, Z. Y. Li, I. El-Kady, R. Biswas and K. M. Ho, *Journal of the Optical Society of America B-Optical Physics*, **20**, 1538-1541 (2003).
12. S. Y. Lin, J. Moreno and J. G. Fleming, *Applied Physics Letters*, **83**, 380-382 (2003).
13. S. Y. Lin, J. G. Fleming and I. El-Kady, *Optics Letters*, **28**, 1909-1911 (2003).
14. S. Y. Lin, J. G. Fleming and I. El-Kady, *Optics Letters*, **28**, 1683-1685 (2003).
15. S. Y. Lin, J. G. Fleming and I. El-Kady, *Applied Physics Letters*, **83**, 593-595 (2003).

16. J. G. Fleming, S. Y. Lin, I. El-Kady, R. Biswas and K. M. Ho, *Nature*, **417**, 52-55 (2002).
17. F. Garcia-Santamaria, H. T. Miyazaki, A. Urquia, M. Ibisate, M. Belmonte, N. Shinya, F. Meseguer and C. Lopez, *Advanced Materials*, **14**, 1144-1147 (2002).
18. S. G. Johnson and J. D. Joannopoulos, *Applied Physics Letters*, **77**, 3490-3492 (2000).
19. D. N. Sharp, M. Campbell, E. R. Dedman, M. T. Harrison, R. G. Denning and A. J. Turberfield, *Optical and Quantum Electronics*, **34**, 3-12 (2002).
20. Y. Yin, Z.-Y. Li and Y. Xia, *Langmuir*, **19**, 622-631 (2003).
21. Y. Fink, A. M. Urbas, M. G. Bawendi, J. D. Joannopoulos and E. L. Thomas, *Journal of Lightwave Technology*, **17**, 1963-1969 (1999).
22. E. Yablonovitch, T. M. Gmitter and K. M. Leung, *Physical Review Letters*, **67**, 2295-2298 (1991).
23. Y. A. Vlasov, X.-Z. Bo, J. C. Sturm and D. J. Norris, *Nature*, **414**, 289-293 (2001).
24. M. Muthukumar, C. K. Ober and E. L. Thomas, *Science*, **277**, 1225-1232 (1997).
25. J. C. Nelson, J. G. Saven, J. S. Moore and P. G. Wolynes, *Science*, **277**, 1793-1796 (1997).
26. A. Sali, E. Shakhnovich and M. Karplus, *Nature*, **369**, 248-251 (1994).
27. T. Martin, U. Obst and J. Julius Rebek, *Science*, **281**, 1842-1845 (1998).
28. N. Bowden, A. Terfort, J. Carbeck and G. M. Whitesides, *Science*, **276**, 233-235 (1997).
29. R. A. Brooks, *Science*, **253**, 1227-1232 (1991).
30. A. vanBlaaderen, R. Ruel and P. Wiltzius, *Nature*, **385**, 321-324 (1997).
31. A. vanBlaaderen and P. Wiltzius, *Advanced Materials*, **9**, 833-& (1997).
32. S. Wong, V. Kitaev and G. A. Ozin, *Journal of the American Chemical Society*, **125**, 15589-15598 (2003).
33. H. Miguez, N. Tetreault, S. M. Yang, V. Kitaev and G. A. Ozin, *Advanced Materials*, **15**, 597-600 (2003).

34. H. Miguez, S. M. Yang and G. A. Ozin, *Langmuir*, **19**, 3479-3485 (2003).
35. H. Miguez, S. M. Yang, N. Tetreault and G. A. Ozin, *Advanced Materials*, **14**, 1805-1808 (2002).
36. S. M. Yang, H. Miguez and G. A. Ozin, *Advanced Functional Materials*, **12**, 425-431 (2002).
37. E. W. Kaler, S. O. Lumsdon, J. P. Williams and O. D. Velev, *Abstracts of Papers of the American Chemical Society*, **223**, D20-D20 (2002).
38. O. D. Velev, K. Bhatt, B. G. Prevo and S. O. Lumsdon, *Abstracts of Papers of the American Chemical Society*, **226**, U479-U479 (2003).
39. M. Nagy and A. Keller, *Polymer Communications*, **30**, 130-132 (1989).
40. O. Cayre, V. N. Paunov and O. D. Velev, *Journal of Materials Chemistry*, **13**, 2445-2450 (2003).
41. O. Cayre, V. N. Paunov and O. D. Velev, *Chemical Communications*, 2296-2297 (2003).
42. Y. Lu, Y. Yin and Y. Xia, *Advanced Materials*, **13**, 271-274 (2001).
43. Y. Lu, Y. Yin and Y. Xia, *Advanced Materials*, **13**, 415-420 (2001).
44. H. R. Sheu, M. S. Elaasser and J. W. Vanderhoff, *Abstracts of Papers of the American Chemical Society*, **196**, 252-Pmse (1988).
45. A. T. Skjeltorp, J. Ugelstad and T. Ellingsen, *Journal of Colloid and Interface Science*, **113**, 577-582 (1986).
46. Y. Yin, Y. Lu, B. Gates and Y. Xia, *Journal of the American Chemical Society*, **123**, 8718-8729 (2001).
47. G. A. Ozin and S. M. Yang, *Advanced Functional Materials*, **11**, 95-104 (2001).
48. O. D. Velev and A. M. Lenhoff, *Current Opinion in Colloid & Interface Science*, **5**, 56-63 (2000).
49. J. J. Storhoff and C. A. Mirkin, *Chemical Reviews*, **99**, 1849-1862 (1999).
50. S. O. Lumsdon, E. W. Kaler and O. D. Velev, *Langmuir*, **20**, 2108-2116 (2004).

51. Y. Saado, M. Golosovsky, D. Davidov and A. Frenkel, *Synthetic Metals*, **116**, 427-432 (2001).
52. M. Golosovsky, Y. Saado and D. Davidov, *Applied Physics Letters*, **75**, 4168-4170 (1999).

Chapter 2

SYNTHESIS OF MONODISPERSE POLYMER MICROSPHERES

2.1 Introduction

For the self-assembly of colloidal crystals, monodisperse spherical particles are most often the basic building blocks. These particles naturally assemble into a close packed structure (FCC or HCP) upon gravity sedimentation presuming their interaction potential is sufficiently negligible so that it is simply a packing efficiency problem. While a monodisperse spherical particle serve as the basic unit in simple, close packed colloidal crystals, more than one size may be used to assemble more complex building blocks analogous to the non-trivial basis in more complex crystal structures. The method for assembling these building blocks in this thesis relies on the precision capture of the spheres in a template. Therefore, monodispersity is an important criterion within each sized sphere population to assemble uniform, complex building blocks.

The desired attributes of the basic spherical particles are the following: easy to synthesize with controlled surface chemistry, inexpensive, and controllable size.

Colloidal polymer particles have been synthesized from numerous compositions with a wide variation in size and monodispersity. Minimization of interfacial energy during growth most often causes particles to adopt a spherical geometry. Polymer particles are commonly synthesized^{1,2} through suspension³⁻⁵, emulsion^{6,7} and dispersion⁸⁻

¹¹ polymerization. Suspension polymerization produces particles of size from 10 μm to 2 mm; emulsion polymerization generates particles of size up to 1-2 μm ; particles from 1 μm to 10 μm can be synthesized through dispersion polymerization and a very narrow size distribution can be obtained. An additional feature of polymer is the T_g , which facilitates fusing the spherical particles into a complex building block.

The diameters of constituent monodisperse particles determine the dimension of the fabricated building blocks. In this thesis, the assembly of complex building blocks with directional bonding properties was the major focus and less attention was focused on the ultimate goal of producing PBG crystals. Thus, the choice of particle size was dictated by the minimal feature size achievable with readily available photolithography facilities available at OSU; namely, a contact mode aligner (Kasper 2001 Wafer Alignment Systems, Kasper Instrument, Mountain View, CA) that consistently delivers feature sizes of 5 μm and above. Thus, the diameter of synthesized polymer particles was chosen to be around 5 μm or larger. If state-of-the-art photolithography facilities were to be used, the feature size could be easily scaled down to sub-micron range. The remainder of this chapter will focus on preparation of the spherical particles in this size range.

Almog, Reich, and Levy¹² have successfully prepared monodisperse polymer particles in the range of 1-6 μm using a dispersion polymerization route. They used a polymeric steric stabilizer in combination with an electrostatic co-stabilizer. Likewise, a successive seeding method used by Vanderhoff^{13,14}, a swelling method used by Ugelstad¹⁵ and various other methods¹⁶⁻¹⁹ have been demonstrated to produce monodisperse particles; however, these methods are complicated, time consuming, and

not effective on preparing batches with high particle concentration as are needed for the large quantities needed in this project.

Ober²⁰ synthesized monodisperse polystyrene particles with diameter from 3 μm to above 10 μm in a dispersion method, using ethylene glycol and ethanol as the dispersion medium and the non-ionic cellulosic derivative, hydroxypropyl cellulose (HPC), as a steric stabilizer. The resultant polymer particles were reported to be uniform in size or, depending on the solvency of the dispersion medium, to have a wider but well-defined particle size range.

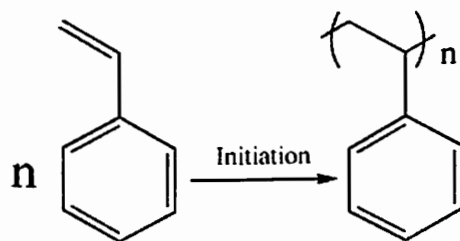


Figure 2.1 Free radical polymerization of styrene as in suspension, emulsion and dispersion polymerization

The dispersion polymerization process reported in this work is similar to Ober's, except that a benign solvent 1-methoxy-2-propanol was used, instead of ethylene glycol due to the hazardous nature, to dissolve the HPC stabilizer in this work.

Addition of ethanol to 1-methoxy-2-propanol enables the preparation of polystyrene particles range from 3 to 10 μm . The ratio of the monomer to dispersion medium as well as the proportion of 1-methoxy-2-propanol to ethanol was studied. The effect of different amounts of stabilizer and initiator added on particle size and monodispersity was also investigated.

2.2 Experimental

2.2.1 Materials

Styrene monomer (99.0 %, 85960-2.5L), 1-methoxy-2-propanol (99.5 %, 484407-4L) and benzoyl peroxide (BPO) (97.0%, 179981-50G) were supplied by www.sigmaaldrich.com. Absolute ethanol was from Pharmco. HPC, with molecular weight (MW) 60,000 (catalog # 401) and 100,000 (catalog # 402), was purchased from Scientific Polymer Products, Ontario, NY. Light mineral oil was from www.fisherscientific.com. Styrene was vacuum distilled before use. The other chemicals were used without further purification. A nitrogen blanket was provided during the polymerization processes.

2.2.2 Instrumentation

Temperature was controlled during the reaction via a controller, OMEGA CN9212A with mechanical relay and 3-wire RTD probe (OMEGA Engineering, INC., Stamford, Connecticut) connected to a heating coil immersed in an oil bath along with the reaction flask. A centrifuge, Eppendorf 5804 with fixed-angle rotor F-34-6-38, (Brinkmann, Westbury, NY) was used for purification and fractional centrifugation of monodisperse polymer particles. A scanning electron microscope JEOL JSM-6360, a scanning-transmission electron microscope JEM 100-CX II (JEOL USA, Inc., Peabody, MA), and an optical microscope Leica DMIRB (Leica Microsystems Inc., Columbia, MD) were used to characterize the size of particles.

2.2.3 Particle Synthesis

To study the factors influencing the diameter and monodispersity of the particles, reaction temperature, dispersion medium composition, initiator and stabilizer concentration were varied in different batches. A typical procedure to synthesize monodisperse polystyrene particles with diameter around 6.4 μm is highlighted as an example. First, 2 g HPC (MW = 60,000) was added into a 250 mL 3-necked distilling flask. Next, 50 mL absolute ethanol and 35 mL 1-methoxy-2-propanol were poured in to form the dispersion medium. Steady magnetic stirring was applied without formation of bubbles in the solvent phase. The oil bath was heated gradually over a 5-10 minute span and kept at 65°C. A reflux condenser was used to trap escaping vapors of ethanol and 1-methoxy-2-propanol. A nitrogen blanket was provided during the whole polymerization process. A schematic illustration of the three-neck flask, condenser, oil bath, and stir plate is in Figure 2.2.

After the HPC was fully dissolved (as observed visually), 15 mL styrene monomer containing 1 g of dissolved BPO was quickly poured into the flask. Within minutes, the medium turned from translucent to turbid and gradually became milky, indicating formation of polystyrene particles. Two hours after initiation of polymerization, the temperature of oil bath was raised to 75°C. Subsequently, polymerization was allowed to proceed for another 22 hours with temperature maintained within the range of 74-76°C. Finally, the reaction medium was cooled to ambient room temperature. During the whole process, the reaction flask and reflux condenser were both sealed with rubber plugs, so that the solvents ethanol and 1-methoxy-2-propanol were kept from escaping.

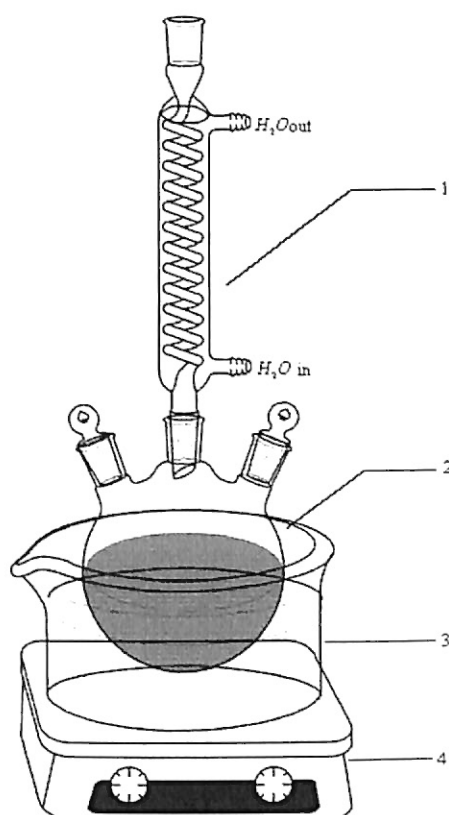


Figure 2.2 Dispersion polymerization apparatus: (1) reflux condenser, (2) 3-necked distilling flask with nitrogen blanket, (3) mineral oil bath with magnetic stirring and heating coil, (4) hot plate

In order to purify the polystyrene particles synthesized, an excess amount of HPC and low molecular weight polystyrene chains in the medium were removed by adding 15 mL of the synthesized dispersion to 30 mL ethanol in a 50 mL centrifuge tube and centrifuged for 3 minutes at speed around 700 rpm, i.e. relative centrifugal force (rcf) 12. The turbid supernatant containing the excess HPC and low molecular weight polystyrene was decanted and white pellet containing the polystyrene particles was retained. 45 mL absolute ethanol was added to the centrifuge tube to re-disperse the particles, after which the same centrifugation/re-dispersing steps were repeated twice.

2.2.4 Separation and Filtration

Although parameters of the dispersion polymerization process could be adjusted to optimize the monodispersity, there were always outlier particles larger and smaller than required in the dispersion. Fractional centrifugation and membrane filtration were used to narrow the particle size distribution.

Equation 2.1 indicates the settling velocity of a rigid particle in a liquid medium of lower density:

$$V = \frac{1}{18} d^2 (\rho_s - \rho_o) \frac{10^{-6}}{h} G \quad (2.1)$$

where

V — the calculated settling velocity (cm/sec),

d — the diameter of the particle (cm),

ρ_s — the density the particle (g / cm^3),

ρ_o — the density of the liquid medium (g / cm^3),

h — the medium viscosity (poise)

G — the relative centrifugal force (rcf) applied.

With appropriate settling distance and rcf, particles of different sizes settled at different velocities accordingly, which led to partition of particles along the settling distance. Big particles settle faster to the bottom of the centrifuge tube while small particles remain in the liquid phase. Typically for the $6.4 \mu\text{m}$ microspheres, 35 mL ethanol and 15 mL of re-dispersed particles in ethanol were added to a 50 mL centrifuge tube and then centrifuged for 2 minutes at $\text{rcf} = 5$. The sediment was separated from the

liquid phase by decanting the turbid supernatant. Subsequently, the sediment of particles was re-dispersed in 50 mL absolute ethanol. This centrifugation, decanting and re-dispersion process was repeated 3-4 times, after which most of the small outlier particles were removed. A membrane filtration step using 5 μm pore size filter (Part # 145828, Part # 145816, Spectrum Laboratories, Rancho Dominguez, CA) in combination with a stir cell is optional to further remove small outlier particles.

The large outlier particles, Figure 2.3b, which had been retained in the sediment during centrifugal separation, were removed via membrane filtration with an 8 μm pore size filter (Part # 145815, Spectrum Laboratories, Rancho Dominguez, CA). The 6.4 μm purified monodisperse polystyrene particles are shown in Figure 2.3a, 2.3c, and 2.3d. The concentration of outliers (small and large) was low in most cases and the centrifugation successfully removed these minority particles.

2.3 Results and Discussion

Particle size and monodispersity control is a function of several thermodynamic and kinetic factors, which include monomer-polymer solubility, reactant composition, dispersion medium etc. Temperature influences the kinetics of initiator decomposition, which in turn determines the rate of polymerization and particle nucleation; and affects the thermodynamic factors, e.g., the solvency of the dispersion medium for polystyrene, which increases as the temperature of the reaction increases. Larger polystyrene particles will be formed generally at higher temperature. On the other hand, a change to the kinetics of the radical chain polymerization due to temperature variation may lead to a widening of the particle size distribution. An oil bath with temperature control, i.e. 65°C

for 2 hours and then 75°C overnight, was necessary to obtain monodisperse PS microspheres. Due to our crude temperature control device some fluctuation in temperature occurred over approximately a 2°C range; however the effect of this variation on monodispersity was not quantified. In general, large temperature fluctuations will lead to a wide particle size distribution and precise temperature control is desirable.

The example procedure described in the experimental section led to monodisperse polystyrene particles of mean diameter 6.4 μm , Figure 2.3. By adjusting ethanol/1-methoxy-2-propanol ratio and using a consistent temperature control scheme, batches of monodisperse polystyrene microspheres ranging from 3.5 to 7 μm were synthesized. Since ethanol is a poorer solvent for polystyrene than 1-methoxy-2-propanol, decreasing the amount of ethanol while increasing that of 1-methoxy-2-propanol correspondingly results in an increase in the size of polystyrene particles synthesized. However, when the ethanol/1-methoxy-2-propanol ratio was below 45/40, polydisperse microspheres were produced. Table 2.1 summarizes the average particle size as observed by microscope analysis for several reaction conditions. Note the increase in particle size with decreasing ethanol/1-methoxy-2-propanol ratio. Figure 2.4 shows SEM images of the particles produced by the various reaction conditions in Table 2.1 after fractional centrifugation.

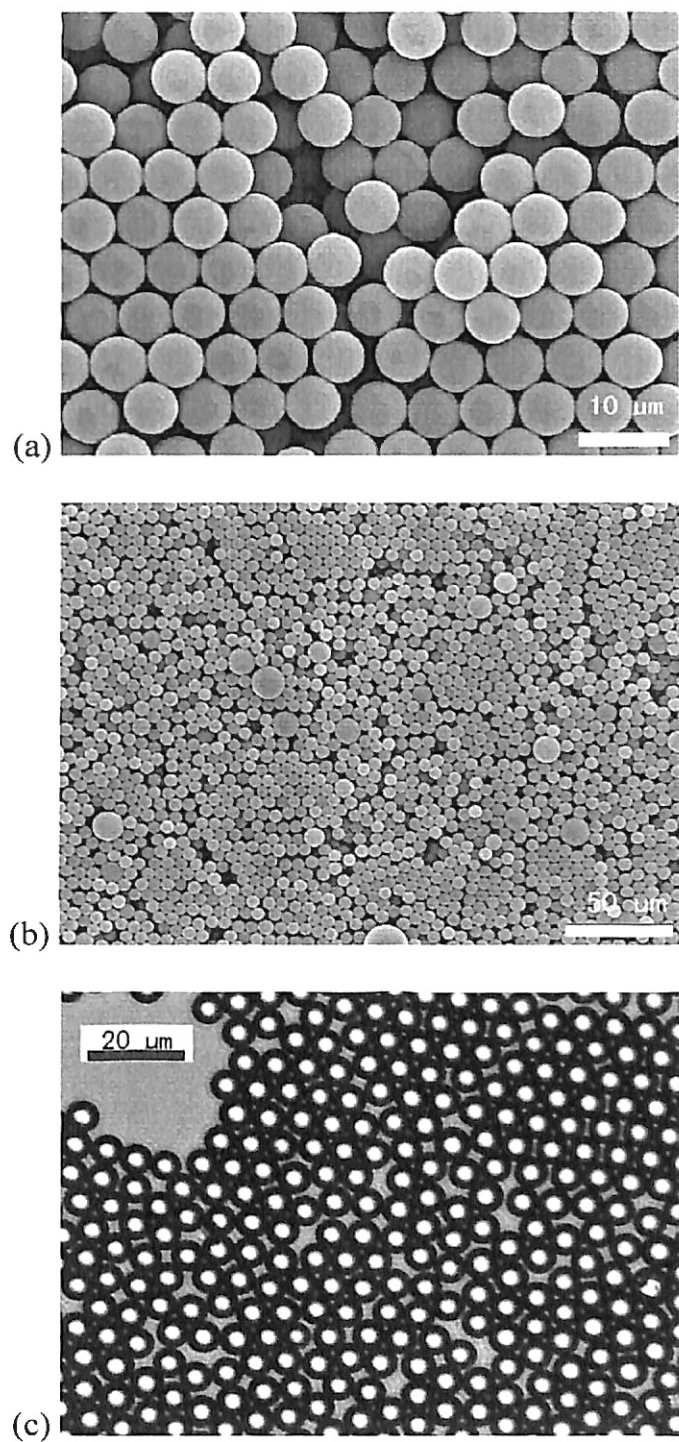


Figure 2.3 Polystyrene particles synthesized through dispersion polymerization (a) SEM image of sputter-coated 6.4 μm polystyrene microspheres, (b) SEM image of sputter-coated 6.4 μm polystyrene particles with large outliers, (c) optical image of 6.4 μm polystyrene microspheres

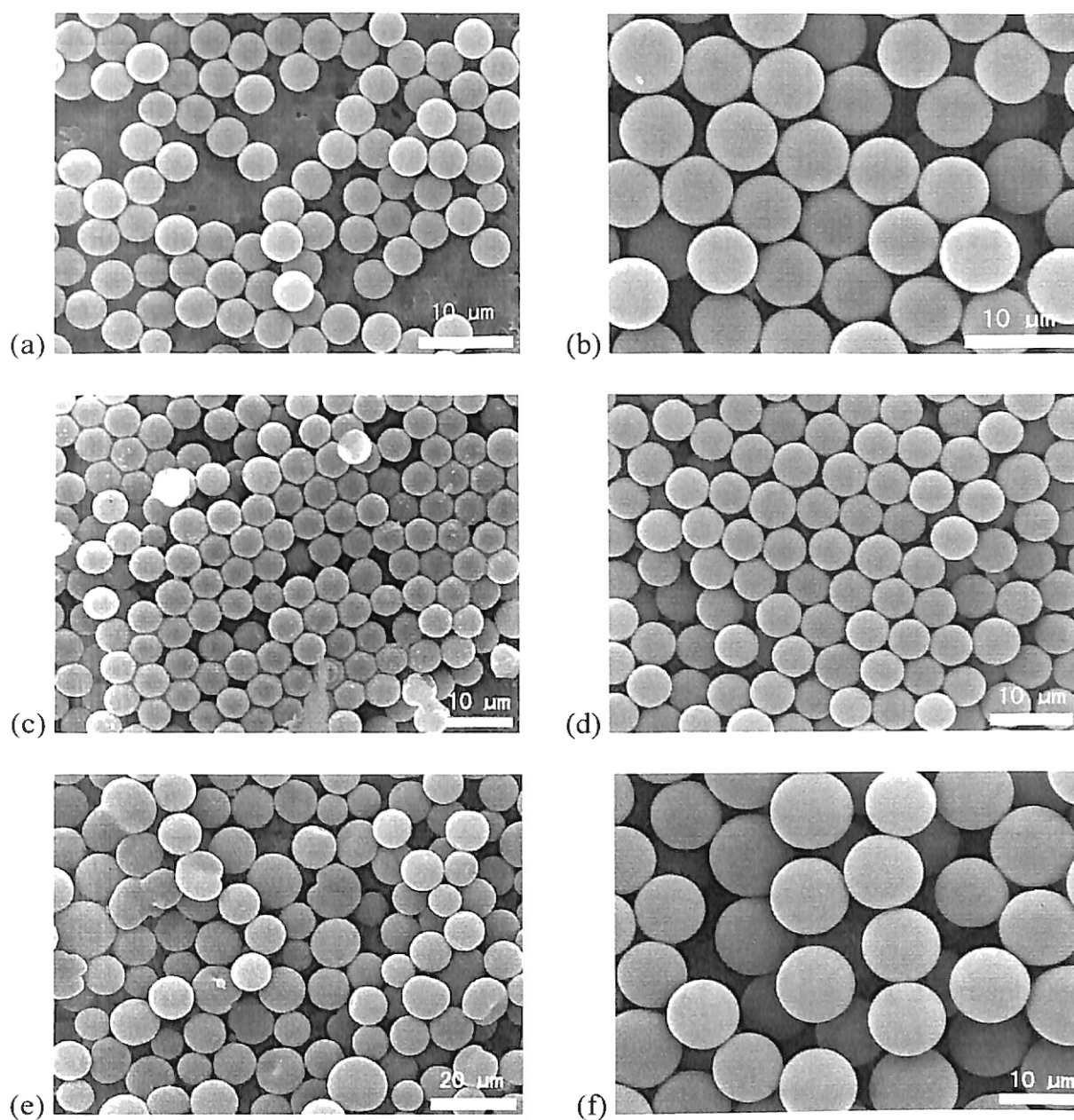


Figure 2.4 SEM images of sputter-coated polystyrene particles synthesized at different ethanol/1-methoxy-2-propanol ratios, where 15 mL styrene monomer, 2 g HPC and 1g BPO were used (a) 60 mL / 25 mL, (b) 50 mL / 35 mL, (c) 47.5 mL / 37.5 mL, (d) 45 mL / 40 mL, (e) 42.5 mL / 42.5 mL, (f) 40 mL / 45 mL

The sizes of the synthesized polymer particles used in this work were examined using JOEL-6360 scanning electron microscope. The size of each sample particle was determined using the lateral dimension measurement function of the Analysis software package coming with the SEM. SAS program was used to calculate the location and variability of the size distribution of the samples. The diameter distribution of the two particles samples to be used in the TASA process is shown in Table 2.2.

Table 2.1 Particle size under different reaction conditions

Styrene (ml.)	Ethanol (ml.)	1-methoxy-2-propanol (ml.)	HPC (g)	BPO (g)	Particle size (μm)
15	40	45	2	1	polydisperse
15	42.5	42.5	2	1	polydisperse
15	45	40	2	1	6-7
15	47.5	37.5	2	1	5
15	50	35	2	1	6.4
15	60	25	2	1	3.8

Table 2.2 Statistical calculations of sizes of the monodisperse polystyrene microspheres

	Number of Particles	Mean (μm)	Median (μm)	Mode (μm)	Std. Deviation (μm)
Sample 50/35/15	229	6.426	6.397	6.287	.219
Sample 60/25/15	176	3.951	3.975	4.006	.321

During the polymerization process, the styrene monomer acted to solubilize the polymer chains; however, its concentration in the medium constantly diminished as

polymerization proceeded. The role that the monomer played in the success of the process was no less important than that of ethanol and 1-methoxy-2-propanol. The final particle size and distribution were influenced by the amount of monomer introduced. Therefore, the volume percentage of styrene monomer was fixed at 15%.

The concentration of stabilizer HPC has a substantial effect on the particle size and monodispersity. When less than adequate stabilizer was used, the particles showed an increased polydispersity as the HPC concentration decreased. In this case, an inadequate amount of stabilizer was adsorbed on the ever-increasing surface area of the particles. Steric stability was destroyed as the attractive force between two particles overcame the stabilization effect. As a result, some particles aggregated. The less stabilizer that was used in that situation, the higher the probability of aggregation and a higher polydispersity was expected. On the other hand, however, excess amount of stabilizer did not noticeably change the particle size and monodispersity. Examples SEM images of polymer particles synthesized with diminishing content of HPC are illustrated in Figure 2.5. HPC with different molecular weights had no evident influence on the particle size and monodispersity. When HPC with higher molecule weight (MW = 100,000) was used instead, identical results were observed if other reaction conditions were remained the same.

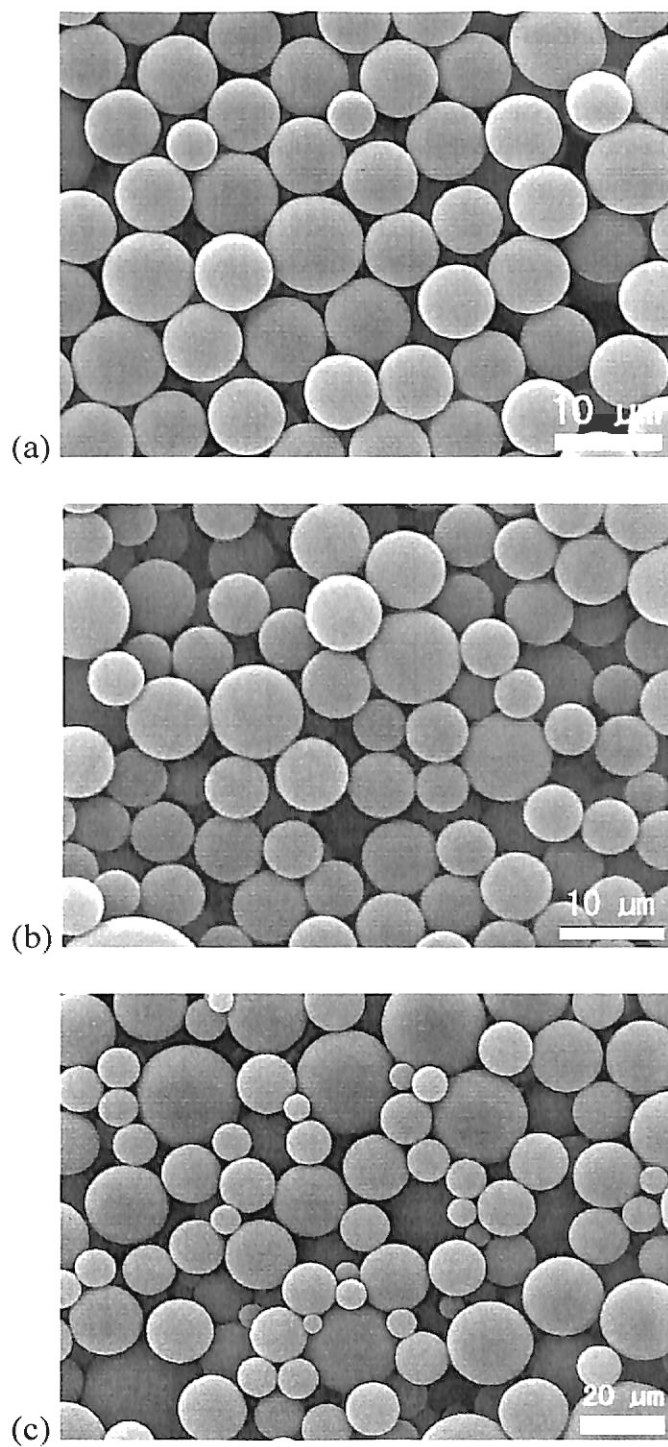


Figure 2.5 SEM images of sputter-coated polystyrene particles synthesized with different stabilizer concentrations, where 15 mL styrene monomer, 47.5 mL ethanol, 37.5 mL 1-methoxy-2-propanol and 1 g BPO were used, (a) 1.5 g HPC, (b) 1.25 g HPC, (c) 1 g HPC

Initiator had a similar effect on the size and monodispersity of polystyrene particles synthesized. When less than adequate initiator was used, the particles showed a slightly increased polydispersity as the BPO concentration decreased. This variation in size was less pronounced than with deficiency in the HPC content as illustrated in Figure 2.6 when compared to Figure 2.5.

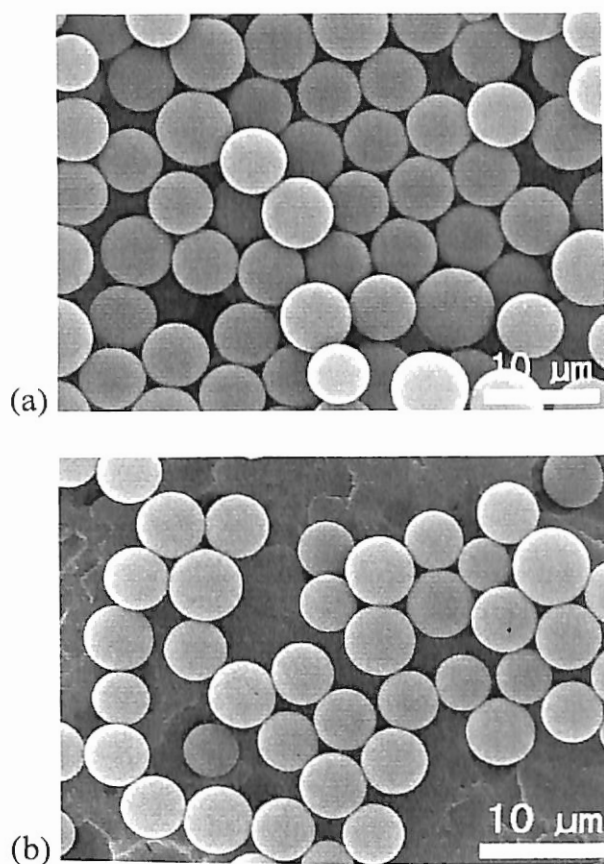


Figure 2.6 SEM images of sputter-coated polystyrene particles synthesized with different initiator concentrations, where 15 mL styrene monomer, 47.5 mL ethanol, 37.5 mL 1-methoxy-2-propanol and 2 g HPC were used (a) 0.75 g BPO, (b) 0.5 g BPO

Repeated cleaning with ethanol did not completely remove the stabilizing HPC molecules attached from the surface of polystyrene particles with a density of

approximately 1.05 g/cm^3 . The precipitated particles could be easily redispersed in ethanol by physical shaking, which facilitated the fractional centrifugation. Fractional centrifugation was effective, but not efficient for removing outlier particles. A major percentage of the total monodisperse particles was sacrificed. However, the method is simple, requiring only repeated centrifugation and decanting. In the future, field flow fractionation (FFF)²¹⁻²³, a technique analogous to liquid phase chromatography, could be used as an efficient alternative to fractional centrifugation.

References

1. J. M. G. Cowie, *POLYMERS: CHEMISTRY & PHYSICS OF MODERN MATERIALS 2nd edition*, 1991.
2. H.-G. Elias, *An Introduction to Polymer Science*, 1997.
3. Y. Konishi, M. Okubo and H. Minami, *Colloid and Polymer Science*, **281**, 123-129 (2003).
4. B. Yang, Y. Kamidate, K. Takahashi and M. Takeishi, *Journal of Applied Polymer Science*, **78**, 1431-1438 (2000).
5. J. M. Hwu, T. H. Ko, W. T. Yang, J. C. Lin, G. J. Jiang, W. Xie and W. P. Pan, *Journal of Applied Polymer Science*, **91**, 101-109 (2004).
6. C. E. Reese, C. D. Guerrero, J. M. Weissman, K. Lee and S. A. Asher, *Journal of Colloid and Interface Science*, **232**, 76-80 (2000).
7. J. Liu, C. H. Chew, L. M. Gan, W. K. Teo and L. H. Gan, *Langmuir*, **13**, 4988-4994 (1997).
8. M. R. Giles and S. M. Howdle, *European Polymer Journal*, **37**, 1347-1351 (2001).
9. N. Behan and C. Birkinshaw, *Macromolecular Rapid Communications*, **22**, 41-43 (2001).
10. W. P. Hems, T. M. Yong, J. L. M. van Nunen, A. I. Cooper, A. B. Holmes and D. A. Griffin, *Journal of Materials Chemistry*, **9**, 1403-1407 (1999).
11. S. P. Armes and R. A. Jackson, *Abstracts of Papers of the American Chemical Society*, **213**, 541-Poly (1997).
12. Y. Almog, S. Reich and M. Levy, *British Polymer Journal*, **14**, 131-136 (1982).
13. E. D. Sudol, M. S. Elaasser and J. W. Vanderhoff, *Journal of Polymer Science Part a-Polymer Chemistry*, **24**, 3499-3513 (1986).
14. E. D. Sudol, M. S. Elaasser and J. W. Vanderhoff, *Journal of Polymer Science Part a-Polymer Chemistry*, **24**, 3515-3527 (1986).
15. S. J. Liang, R. M. Fitch and J. Ugelstad, *Journal of Colloid and Interface Science*, **97**, 336-347 (1984).

16. M. Okubo, T. Yamashita, T. Suzuki and T. Shimizu, *Colloid and Polymer Science*, **275**, 288-292 (1997).
17. M. Okubo, M. Shiozaki, M. Tsujihiro and Y. Tsukuda, *Colloid and Polymer Science*, **269**, 222-226 (1991).
18. M. Okubo and T. Nakagawa, *Colloid and Polymer Science*, **270**, 853-858 (1992).
19. M. Okubo and M. Shiozaki, *Polymer International*, **30**, 469-474 (1993).
20. C. K. Ober and K. P. Lok, *Macromolecules*, **20**, 268-273 (1987).
21. M. E. Miller and J. C. Giddings, *Abstracts of Papers of the American Chemical Society*, **212**, 1-Pmse (1996).
22. J. C. Giddings, *Analytical Chemistry*, **69**, 552-557 (1997).
23. H. Lee, S. Kim, R. Williams and J. C. Giddings, *Analytical Chemistry*, **70**, 2495-2503 (1998).

Chapter 3

SURFACE MODIFICATION OF POLYSTYRENE MICROSPHERES

3.1 Introduction

Monodisperse particles find applications in areas such as biochemistry^{1,2}, catalyst support³ and fluid dynamics⁴. Often, chemical modifications to the particles by covalently linking functional groups to the surface⁵⁻⁸ provide means for defining the chemical and physical properties for the purpose of specific chemical interactions between the particles and the adsorbates such as proteins and cells. Surface modification may also allow colloid chemists to tailor the interaction potentials between particles. In other instances, composite particles may be synthesized by the inclusion of nanoparticles in the synthesis. For example, the physical incorporation of magnetic nanoparticles into larger polymer particles can make the resulting composite particles magnetically responsive^{9,10}. Whether by surface modification or bulk inclusion of responsive nanoparticles, these properties may facilitate manipulating the movement, orientation and spatial arrangement of the particles during a self-assembly process using external fields.

In chapter two, the dispersion polymerization method for the preparation of monodisperse polystyrene microspheres was described. Except for the physically adsorbed HPC stabilizer, and the benzoyl end groups on the polystyrene molecule chains resulting from the decomposed initiator BPO, the polystyrene microspheres possess a

neutral, hydrophobic surface. For the purpose of creating complex building blocks from spherical colloidal particles, chemically distinct particles with covalently grafted functional groups and of different size than the pure polystyrene particles were synthesized. Thus in an assembled structure, the covalently grafted portion of a particle cluster is functionally distinct from the polystyrene particle by its surface chemistry.

In this chapter, a two-stage dispersion polymerization method for the preparation of the monodisperse amine-functionalized polystyrene microspheres with controllable size is presented. Subsequently, the difference in surface chemistry is demonstrated by the selective adsorption of gold nanoparticles onto the aminated surfaces via electrostatic attraction.

The overall goal of this project was to create complex colloidal building blocks to enable a rational design of self-assembling particles. Beyond simple geometry, bonding between building blocks during the assembly process was envisaged to involve selective interactions between two or more sets of building blocks (i.e., type A bond to type B, but A-A and B-B interactions are unfavorable). As a starting point, two satellite spheres were to be precisely positioned around a central particle as shown in Figure 1.6. Using aminated satellite particles and selective adsorption of a gold nanoshell on each of these particles, thiolized oligonucleotides could then be selectively adsorbed as illustrated in Figure 3.1 to provide a route for easily controlling the colloidal self assembly process.

Gold particles synthesized from wet chemistry methods generally fall into nano-size range^{3,12,13}. As the size increases further, the attractive force between Au nanoparticles overcomes stabilization effect and aggregation occurs. The effective charge on the Au nanoparticles is negative and they can be made to adsorb on the

positively charged aminated-polystyrene surfaces. The size of the Au nanoparticles and the thickness of the adsorbed Au nanoparticle layer are negligible compared with the diameter of the polymeric core. Under appropriate conditions, the adsorbed nanoparticles can form a continuous layer of gold in the form of a nanoshell. ^{3,12,13}, and a polymeric protecting layer is added to stabilize the Au nanoshell particles.

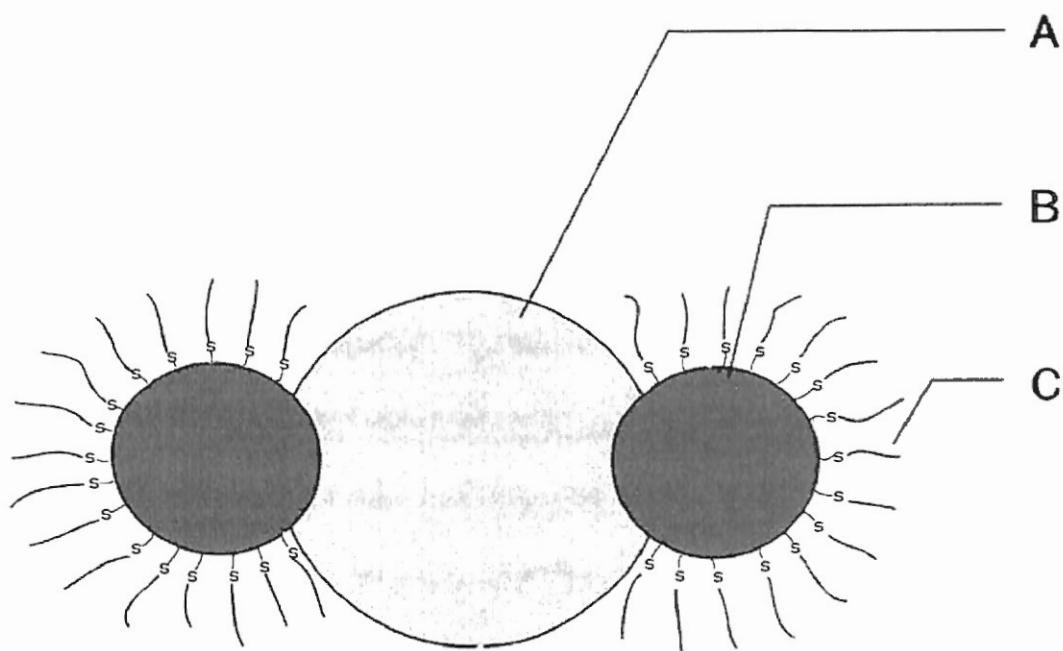


Figure 3.1 Schematic illustration of a triplet building block to be self-assembled: A—the polystyrene microspheres at the center, B—the amine-functionalized particles with gold nanoshells, C—the thiolized oligonucleotides attached to the Au particles through the gold-thiol binding

Amine-functionalized polystyrene particles with positive surface charge have been synthesized in many ways¹⁴⁻¹⁸. V. L. Covolan demonstrated the preparation of aminated polystyrene latexes through copolymerization of styrene and Boc-p-

aminostyrene^{2,19}, however the control over particle size and monodispersity were not of major interest in his work. To synthesize monodisperse amine-functionalized polystyrene particles with desired size, the most direct route of synthesis may appear to be the simple copolymerization of styrene blended with Boc-p-aminostyrene monomer, followed by a de-protection step. Often, it is only the surface that needs to be functionalized, and optimizing a new chemistry using dispersion polymerization is time-consuming. Instead of using copolymerization for the entire particle, a modified two-stage dispersion polymerization technique has been proposed to get controlled particle size and desired surface functionality.

The two-step process of creating only a surface layer of co-monomer on a polystyrene substrate is schematically illustrated in Figure 3.2. In the first step, the dispersion polymerization of styrene monomer is conducted to establish the polystyrene substrate particles with desired size and monodispersity; in the following step, Boc-p-aminostyrene is to be added into the reaction medium, before the termination of polymerization, to form a very thin polystyrene/Boc-p-aminostyrene copolymeric layer on the surface of existing polystyrene microspheres, which bears amine groups after a de-protection step.

The remainder of this chapter discusses the two-stage preparation and chemical treatment method to generate amine groups on the copolymeric particle surface, and the initial experiments for selectively adsorbing Au nanoparticles on amine-functionalized polystyrene particles while avoiding adsorption onto the plain polystyrene particles. The effect of stabilizer and surfactant on the successful adsorption of Au nanoparticles is briefly discussed.

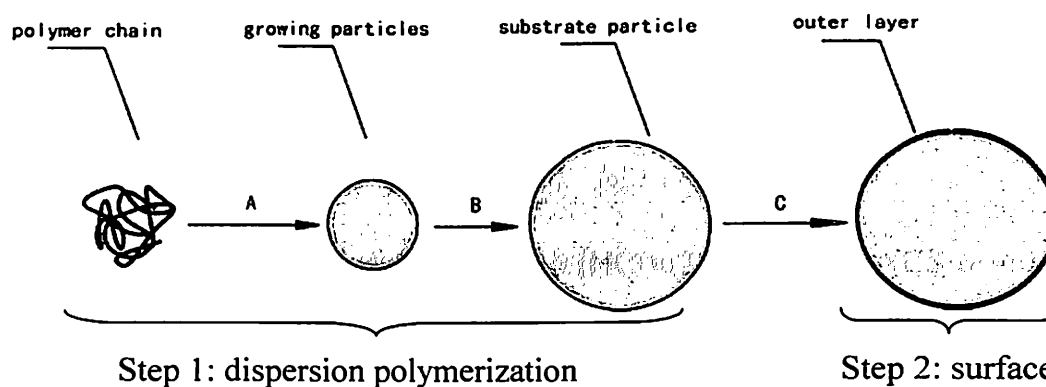


Figure 3.2 Schematic illustration of the two-stage dispersion polymerization technique: A—formation of polystyrene microspheres from precipitated polymer chains, B—size growth of the substrate polystyrene microspheres, C—formation of a copolymeric layer on the surface of existing polystyrene substrate

3.2 Experimental

3.2.1 Materials

Monomer Synthesis: 1,4-dioxane (99+%, 36048-1) and di-tert-butyl pyrocarbonate (98%, 34660-25G) were purchased from SigmaAldrich, Milwaukee, WI. 4-aminostyrene (96%, 001223-25G) was supplied by Oakwood Products, West Columbia, SC. Ethyl acetate (HPLC, reagent grade ACS) and n-hexane (35900HPLC, ACS grade) were supplied by from Pharmco, Brookfield, CT.

Two-Stage Dispersion Polymerization: Styrene monomer (99.0 %, 85960-2.5L), 1-methoxy-2-propanol (99.5+%, 484407-4L) and BPO (97.0%, 179981-50G) were purchased from SigmaAldrich, Milwaukee, WI. Absolute ethanol (anhydrous, ACS grade) was supplied by Pharmco, Brookfield, CT. HPC (MW 60,000 and 100,000) was purchased from Scientific Polymer Products, Ontario, NY. Light mineral oil (0121-4.

paraffin oil) for oil bath was supplied by Fisher Scientific, Fair Lawn, NJ. Styrene monomers were distilled under nitrogen blanket. Other chemicals were used without further purification.

Surface Treatment: Hydrochloric acid (HCl) (284000ACS, ACS reagent grade) was supplied by Pharmco, Brookfield, CT. Sodium dodecyl sulfate (SDS) (98%, 862010-100G) and 1-methoxy-2-propanol (99.5+%, 484407-4L) were purchased from SigmaAldrich, Milwaukee, WI. Pluronic pastille surfactant F108 (batch WPAY35B) was supplied by BASF, Mt. Olive, NJ. Sodium hydroxide (S1295, 500G) was supplied by Spectrum, New Brunswick, NJ.

Synthesis of Au Nanoparticles: Sodium citrate (S4641-500G) and hydrogen tetrachloroaurate trihydrate ($\text{HAuCl}_4 \cdot 3\text{H}_2\text{O}$) (99.9%, 520918-1G) were purchased from SigmaAldrich, Milwaukee, WI. Tetrakis(hydroxymethyl)phosphonium chloride (THPC) (80%, aqueous, T06475-100GM) was purchased from Pfaltz & Bauer, Waterbury, CT. Formaldehyde (37% w/w aqueous) and potassium carbonate (P1235, 500G) were supplied by Spectrum, New Brunswick, NJ.

3.2.2 Synthesis of Boc-p-Aminostyrene Comonomer

The synthesis of Boc-p-aminostyrene was carried out using the procedure outlined in Covolan's work². First, 5 mL 4-aminostyrene (96%), used without purification, was dissolved in 100 mL 1,4-dioxane and poured into a 250-mL three-necked flask, which was equipped with a reflux condenser, magnetic stirring and cooled with a water/ice bath. Next, a solution of 0.055 mol di-tert-butyl dicarbonate in 25 mL 1,4-dioxane was added under nitrogen atmosphere. The solution was stirred overnight under nitrogen blanket

and then concentrated by vacuum evaporation of 1,4-dioxane. The reaction is shown in Figure 3.3. The resulting solid product was dissolved in ethyl acetate, then a dilute HCl aqueous solution was added to get pH = 5. The organic phase was separated and evaporated. The obtained crude Boc-p-aminostyrene was re-crystallized from n-hexane to yield crystalline grains of Boc-p-aminostyrene monomer. Due to the existence of colored impurities in the 4-aminostyrene, the product monomer was slightly yellow.

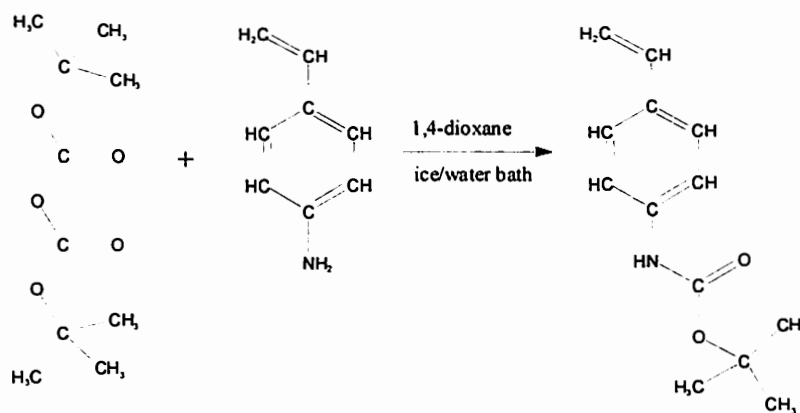


Figure 3.3 Protection of amine group on 4-aminostyrene using di-tert-butyl dicarbonate

3.2.3 Two-Stage Dispersion Polymerization

In a typical procedure to synthesize monodisperse amine-functionalized particles with size around 4 μm , dispersion polymerization of styrene monomer was initiated in the first step, similar to the process described in chapter two. 1 g HPC (MW = 60,000) was first added into a 250 mL 3-necked distilling flask. Next, a mixture of 35 mL absolute ethanol and 7.5 mL 1-methoxy-2-propanol was added to the reaction vessel. Steady magnetic stirring was applied without forming bubbles in the solvent phase. The oil bath was heated in 5-10 minutes and kept at 65°C. A reflux condenser was used to

trap escaping vapors of ethanol and 1-methoxy-2-propanol. A nitrogen blanket was provided during the whole polymerization process. After the HPC was fully dissolved (as observed visually), 7.5 mL of styrene monomer containing 0.5 g of dissolved BPO was quickly poured into the flask. Immediately, the medium became turbid and then gradually became milky, indicating the formation of polystyrene particles. Two hours after the initiation of polymerization, the temperature of the oil bath was raised to 75°C. 16 hours after the reaction temperature was raised, the polystyrene microspheres in the dispersion presumably had almost reached their final diameter and a solution of 0.3 g Boc-p-aminostyrene in 3.5 mL ethanol and 0.75 mL 1-methoxy-2-propanol was quickly poured into the reaction medium. The ratio of ethanol/1-methoxy-2-propanol added was kept consistent with that of the polymerization medium used in the first step. 6 hours later, the reaction flask was cooled to ambient room temperature. The copolymerization reaction is illustrated in Figure 3.4.

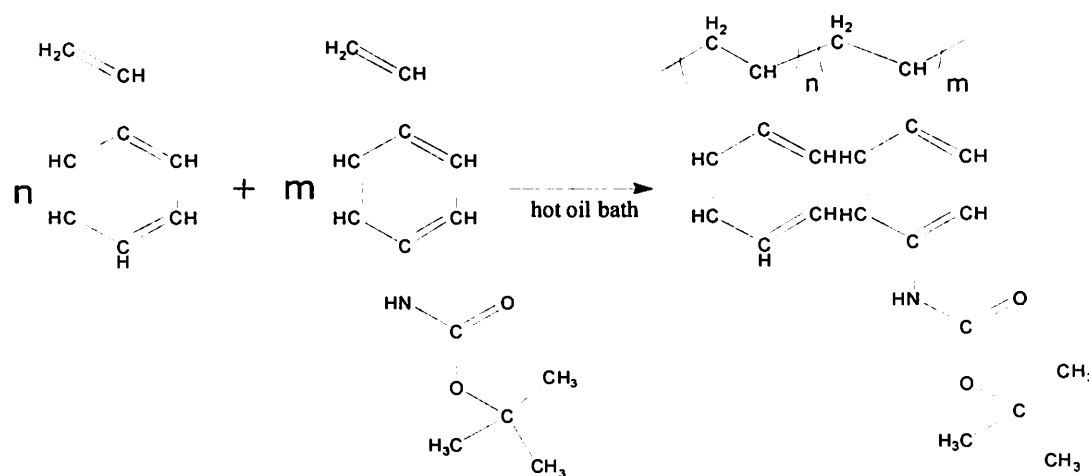


Figure 3.4 The copolymerization of the styrene monomer and the Boc-p-aminostyrene monomer

3.2.4 Acidic Cleavage

Ionized amine groups on the outer layer of the particles synthesized through the two-stage method can be exposed by acidic cleavage of protecting groups on polystyrene/Boc-p-aminostyrene copolymer, as illustrated in Figure 3.5.

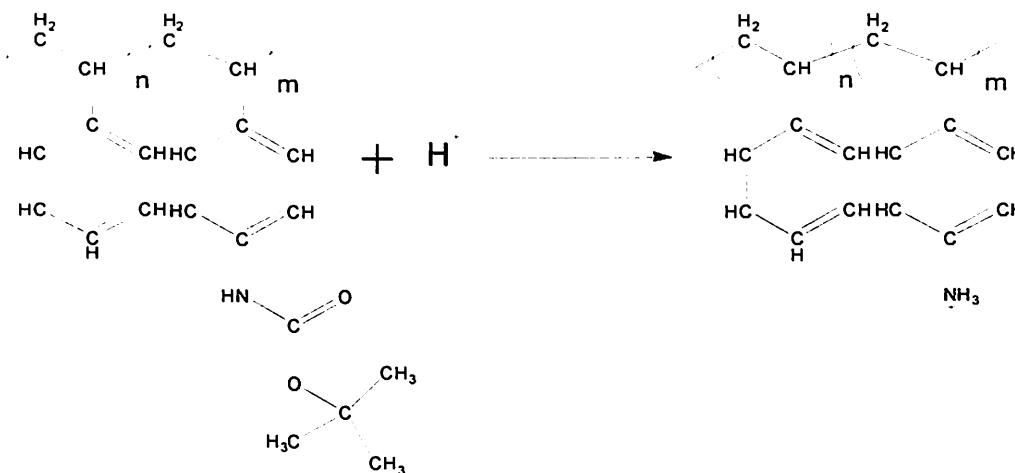


Figure 3.5 Generation of the ionized amine groups on the polystyrene/Boc-p-aminostyrene copolymeric particles through acidic cleavage

The description of the detailed processing steps for the de-protection of amine groups on the polystyrene/Boc-p-aminostyrene copolymeric particles is deferred to section 3.2.6 so that it is in the proper context with the description of electrostatic adsorption of gold nanoparticles on the amine functionalized polymer particles.

3.2.5 Synthesis of Au Nanoparticles

Au nanoparticles can be synthesized through reduction of dilute hydrogen tetrachloroaurate solution in the presence of a stabilizing species. When sodium citrate is used as the reducing agent, the resulting Au nanoparticles are of size around 20-30 nm or

larger. N. J. Halas used THPC aqueous solution to reduce hydrogen tetrachloroaurate and synthesized much smaller Au particles around 1-3 nm. In the current work, batches of different-sized Au nanoparticles were prepared and used to compare their adsorption performance on the amine-functionalized polystyrene particles.

3.2.5.1 Sodium Citrate Reduction

A solution of 1% (w/v) $\text{HAuCl}_4 \cdot 3\text{H}_2\text{O}$ (1 mL, 0.5 M) was diluted to 100 mL (5×10^{-4} M) with DI water and heated to boil with reflux condenser in air. A 1% aqueous sodium citrate solution (2.5 mL) was added to the refluxing gold solution. After continued refluxing for about 20 min, the solution (initially pale yellow) turned first purple and finally red, indicating the presence of gold nanoparticles. The red solution was refluxed for an additional 10 min and cooled and stored for later use.

3.2.5.2 THPC reduction

To a 45 mL aliquot of DI water, 0.5 mL of 1 M NaOH and 1 mL of THPC solution (prepared by adding 12 μL (0.067 mmol) of 80% THPC in water to 1 mL of HPLC grade water) was added. The reaction mixture was stirred for 5 min with a strong vortex, after which 2.0 mL (27 mmol) of 1% HAuCl_4 in water was added quickly to the stirred solution. The dark brown color of the resulting solution indicated the formation Au colloids. By variation of the volume of 1% HAuCl_4 added, the size of the gold colloid particles could be varied. For example, a change from 2.0 mL to 1.5 mL led to a reduction in the diameter of the nanoparticles from 2-3 nm to 1-2 nm. In the work

described below, colloidal gold particles that were 2-3 nm in diameter were utilized, which were routinely obtained using the THPC reduction procedure outlined above.

3.2.6 Stabilizer Exchange on Polystyrene and Aminated Polystyrene Particles

The following is an example of the process to remove HPC stabilizer on the polymer particles and replace it with Pluronic F108. 3 mL dispersion directly from the polymerization flask was initially added to a 50 mL centrifuge tube. Subsequently, 20 mL ethanol was added to the tube and it was vigorously shaken. The dispersion was then centrifuged at 2000 rpm for 2 minutes. The supernatant was decanted and the sediment of particles was redispersed in 20 mL ethanol. The same centrifugation, decanting and redispersing were repeated twice to remove excess HPC stabilizer and low molecular weight polymer chains in the medium, after which the particles were dispersed in ethanol where the physically adsorbed HPC served as the stabilizer. Approximately 0.3 g of a Pluronic F108 stock solution, prepared with 21.318 g Pluronic F108 surfactant powder and 36.655 g DI water, was added to the dispersion. A sonication bath was used to assist the dissolution of the F108 solution in the dispersion. Afterwards, 20 mL 1-methoxy-2-propanol, a good solvent for HPC, was added to the dispersion. A vigorous shaking was again applied. Centrifugation of the dispersion at 2000 rpm for 2 minutes was used to separate the polymer particles from the dispersion medium. At this point, the HPC molecules, originally adsorbed on the particles surface, were thought to have been replaced by Pluronic F108 molecules and removed through decanting the supernatant. Thus, to test the hypothesis of stabilizer exchange, the Pluronic needed to perform two

functions: 1) stabilize the particles so that dispersion was easily accomplished and 2) prevent the adsorption of gold nanoparticles in contrast to the HPC.

3.2.7 Adsorption of Au Nanoparticles on Aminated Polystyrene Particles

When polystyrene/Boc-p-aminostyrene particles, stabilized with Pluronic F108 surfactant, were subject to strong acid treatment, amine groups on the outer layer of the polystyrene/Boc-p-aminostyrene copolymeric particles were generated through cleaving the protecting group as described in section 3.2.4, and became positively charged. In a typical process, 3 mL dispersion of polystyrene/Boc-p-aminostyrene copolymeric particles stabilized with Pluronic F108 surfactant added to a 50 mL centrifuge tube. Subsequently, 25 mL ethanol was added, followed by the addition of 2 mL concentrated HCl solution (assay 36.5 - 38.0%). A water bath at 60°C was provided for speeding up the acidic deprotection reactions. After 30 minutes, the dispersion was centrifuged and the supernatant decanted. Then the sediment was redispersed in ethanol, followed by centrifugation and redispersing. At this point, the polymer particles were positively charged.

Simple addition of a solution of Au nanoparticles, with size around 2 nm, to an dispersion of the positively charged aminated polystyrene particles was used for the adsorption of Au nanoparticles. Reversibility of the gold adsorption was tested by increasing the pH of the suspension and thus weakening the electrostatic interaction. Subsequently reduction of pH was used to regenerate the positive nature of the aminated polymer particles and cause re-adsorption of the Au particles.

3.2.8 Gold Nanoshell Growth

To boost the amount of Au coverage on the surface of the aminated polystyrene particles, a gold nanoshell was grown by reduction of HAuCl_4 using the adsorbed nanoparticles as seeds for the growth. 0.125 g of potassium carbonate was added to 500 mL of DI water. After complete dissolution, 20 mL of this solution was added to a 100 mL beaker with magnetic stirring. 0.3 mL 1% HAuCl_4 in DI water was added. The solution initially appeared translucent yellow and slowly became colorless. 0.02 g of SDS was subsequently added as dispersant. Aminated-polystyrene microspheres (0.2% w/w) in 3 mL ethanol/water with adsorbed THPC reduced Au nanoparticles was added to the gold salt solution. After 10 min stirring, 0.05 mL formaldehyde (37% w/w) was added into the gold salt solution. Over the course of 2-4 min, the solution changed from colorless to bluish, indicating the growth of Au seeds and the formation of a gold nanoshell structure. Addition of positively charged polyethylenimine solution (MW 25,000-50,000, 10% w/w) right after the nanoshell formation stabilized the composite particles.

3.3 Results and Discussion

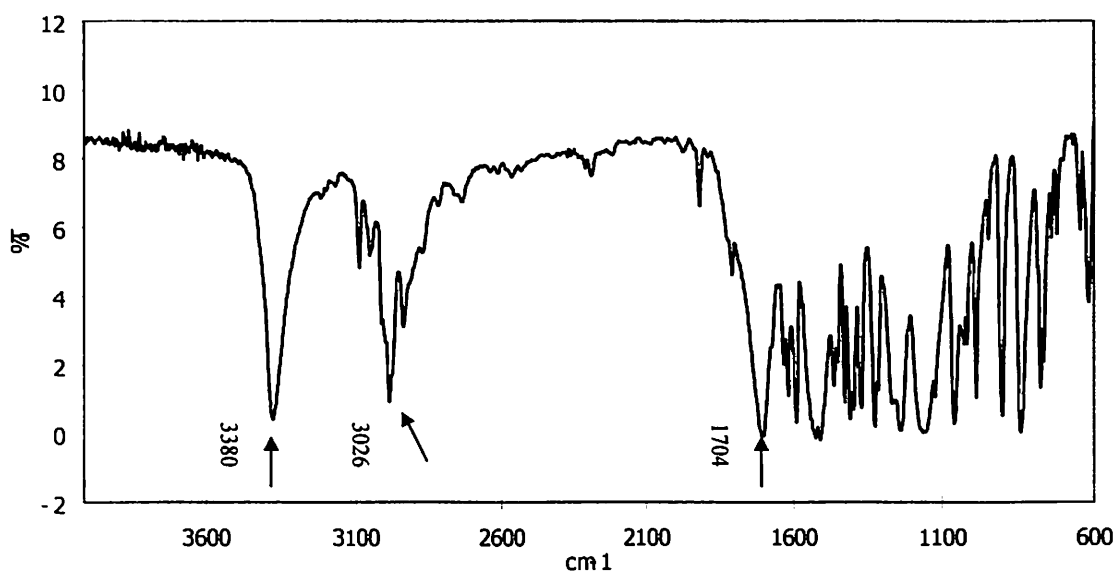
3.3.1 Amine Functionalization of Polystyrene Particles

The amine-functionalized layer derived from the addition of Boc-p-aminostyrene imparted a positively charged surface to the polystyrene despite its relatively small volume fraction. The thin layer and post-synthesis acidic treatment had little effect on the overall size of the particles. Therefore, the diameter and monodispersity of the

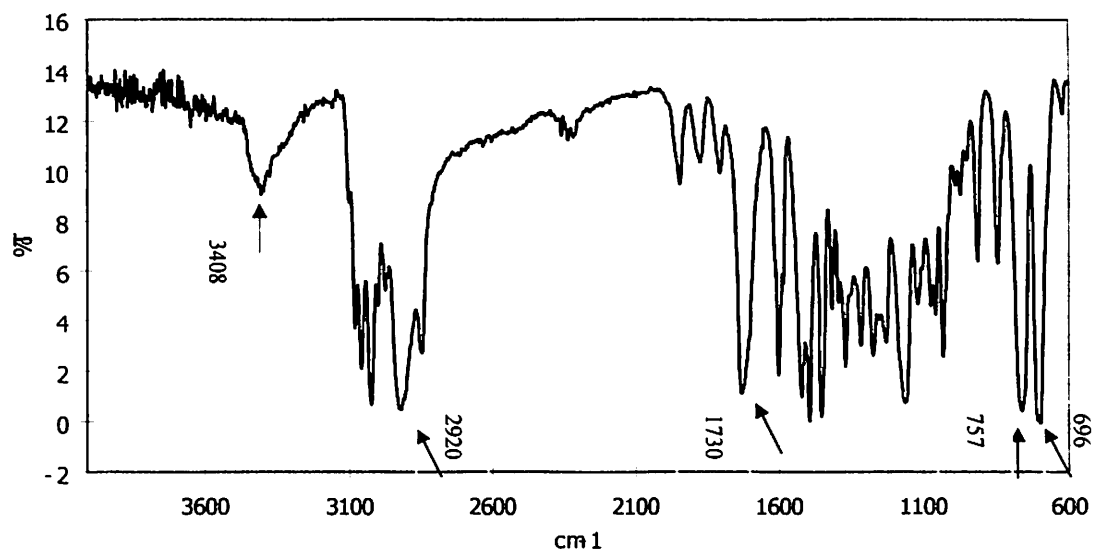
particles were determined in the first step of this synthesis scheme whereas the surface chemistry was modified in the second. This method makes the synthesis of potentially a variety of monodisperse functionalized polymer particles by modifying the comonomer added in the second step quite flexible. It is especially useful when the surface chemistry of the polymer particles and monodispersity are both of interest.

To verify the presence of functional amine groups after the two-step synthesis, FTIR spectra of the Boc-p-aminostyrene monomer and the functionalized polystyrene/Boc-p-aminostyrene particles were analyzed. The FTIR spectra for the Boc-p-aminostyrene monomer is shown in Figure 3.6a and compared to that for the copolymer and amine functionalized polystyrene particles. Each spectrum demonstrates the existence of N-H bond, with absorption peaks at 3380 cm^{-1} , 3408 cm^{-1} and 3400 cm^{-1} respectively. Peaks for the carbonyl group C=O stretching are observed at 1704 cm^{-1} , 1730 cm^{-1} and 1731 cm^{-1} respectively. Characteristic profiles of aromatic ring stretching at 3026 cm^{-1} , C-H stretching at 2920 cm^{-1} and 2849 cm^{-1} are clearly seen. Strong peaks at 696 cm^{-1} and 757 cm^{-1} come from the monosubstituted polystyrene rings are only observed in the copolymer particles, but not in the Boc-p-aminostyrene monomer.

(a) FTIR Spectrum For Boc-p-AMST Monomer



(b) FTIR Spectrum for Copolymer Particles



(c) FTIR Spectrum For PS-NH₂ Particles

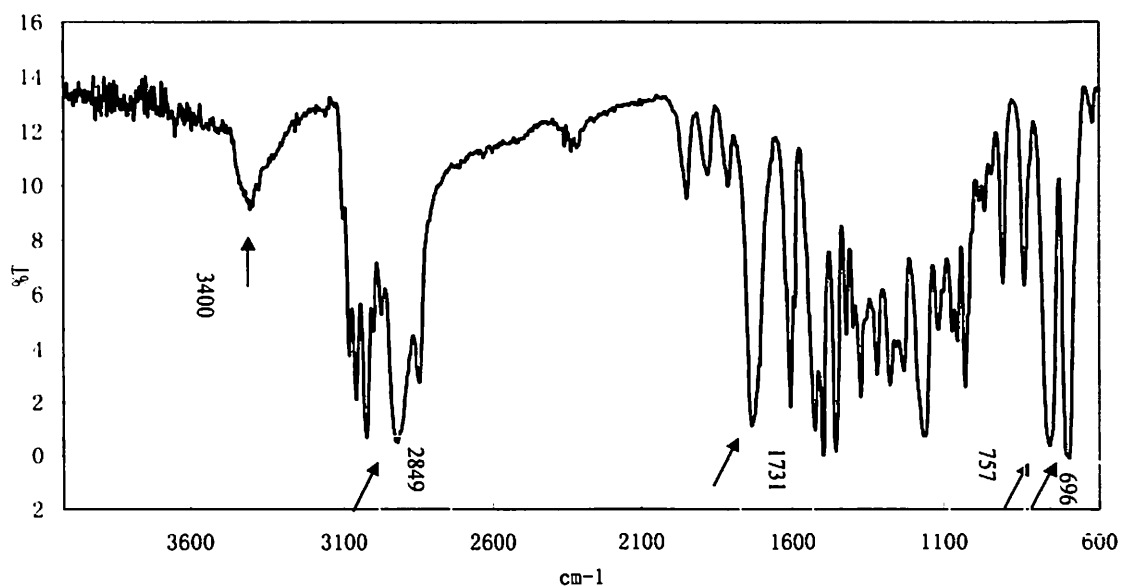


Figure 3.6 FTIR spectra for (a) Boc-p-aminostyrene monomer, (b) functionalized polystyrene/Boc-p-aminostyrene and (c) amine functionalized polystyrene particles

3.3.2 Stabilizer Removal and Exchange

The physically attached HPC molecules could be easily removed from the surface of the polymer particles by using 1-methoxy-2-propanol, a good solvent for HPC. Figure 3.7 illustrates a soft agglomerate of polystyrene particles in ethanol, when the HPC stabilizer molecules were removed by adding 1-methoxy-2-propanol to the dispersion without the addition of a replacement stabilizer such as Pluronic F108. Such agglomeration was typical if a replacement stabilizer had not been added. On the other hand, if a replacement stabilizer was present, such agglomerates were not observed and the particles remained well dispersed.

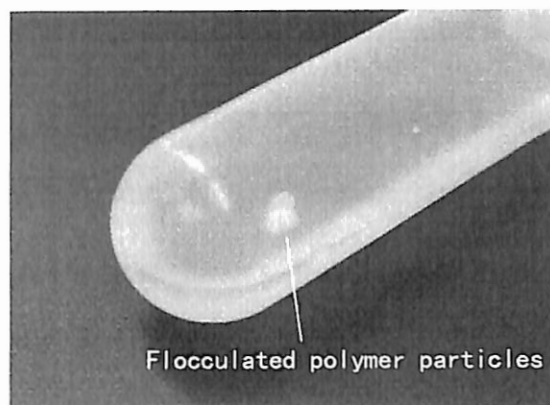


Figure 3.7 Flocculated polystyrene particles in ethanol, when the HPC stabilizer molecules were not available

3.3.3 Gold Nanoparticle Adsorption and Gold Nanoshell Assembly

The adsorption of gold nanoparticles onto the larger polystyrene particles may be accomplished by a number of bonding mechanisms of varying strength. First, attractive van der Waals forces may cause adsorption of the small nanoparticles on the large polystyrene particles. This mechanism may be mitigated by steric hindrance of the stabilizing molecules on both the nanoparticles and the polystyrene. Second, if the stabilizer on the polystyrene is polar, as is necessary to stabilize it in polar solvents, the gold nanoparticles may be adsorbed by weak hydrogen bonding like interactions. Third, if the polystyrene surface or stabilizer is charged oppositely of the gold nanoparticles, electrostatic attraction may occur. In the current case, a mechanism for selectively adsorbing the gold nanoparticles to aminated polystyrene but not to plain polystyrene particles was sought.

To adsorb the negatively charged Au nanoparticles through electrostatic interaction, the polymer particles have to be positively charged. The functionalized

polymer particles carry -NH_3^+ groups on the surface after acidic de-protection as briefly described in section 3.2.4, if the pH is kept near neutral to acidic. However, the existence of the physically adsorbed HPC molecules (stabilizer from dispersion polymerization) on the polymer particles surface complicates the situation. HPC was found to possess enough polar character due to the presence of hydroxyl groups to effect an attractive force (similar to hydrogen bonding, see Figure 3.8) in an acidic conditions and to overcome steric hindrance and adsorb some Au nanoparticles, as shown in the SEM micrograph of Figure 3.9. The surface was not sputter coated with gold for SEM analysis, the nanoparticles are visible as the darker regions on the surface of the otherwise smooth particles, and the brighter patches are uncovered areas.

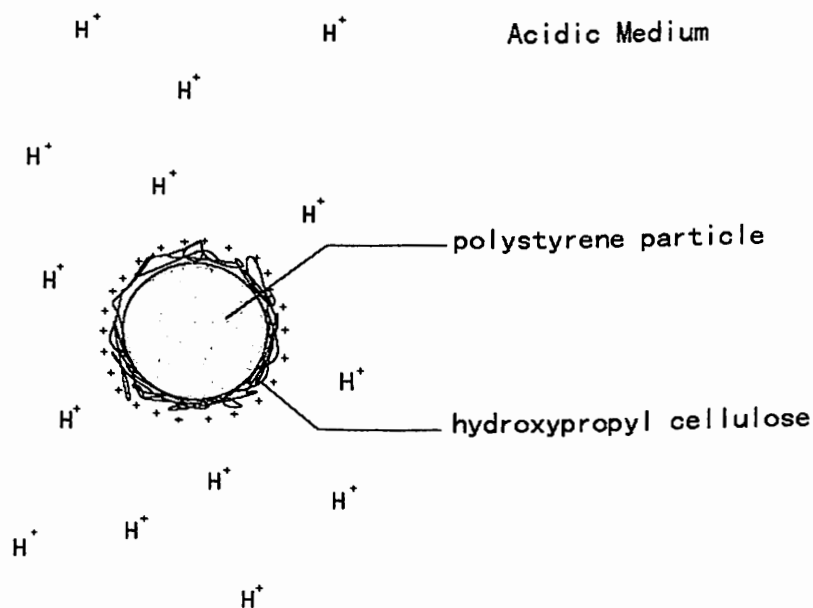


Figure 3.8 Effectively positively charged HPC molecules attached to the surface of a polystyrene particle in acidic solution

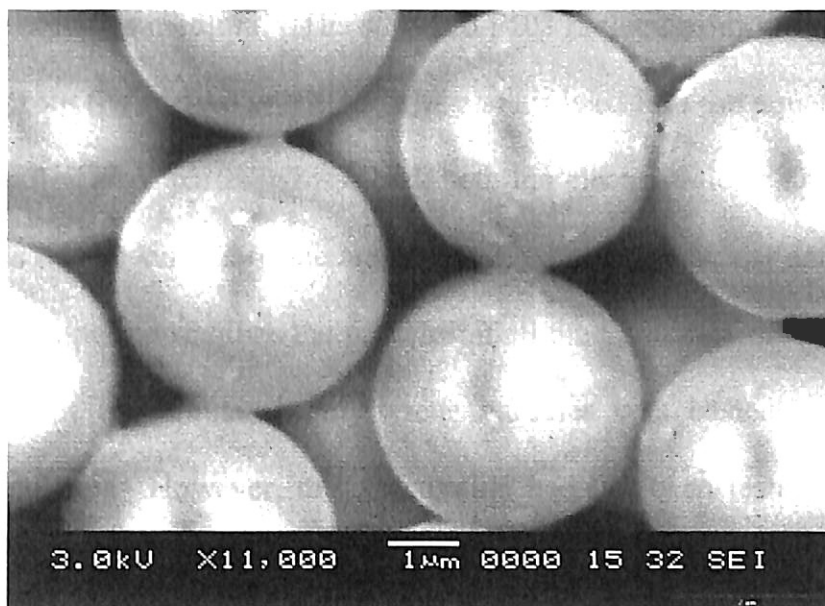


Figure 3.9 SEM images of Au nanoparticles coated HPC stabilized polystyrene particles

Thus, the HPC stabilizer used in the synthesis of the polystyrene and aminated polystyrene obscured the effect of the underlying surface chemistry of the colloidal particles, and, hence, the ability to selectively adsorb gold on specific particles in the assembled clusters. Therefore, the HPC molecules on the polymer particle surface had to be replaced with a nonionic stabilizer that prevented adsorption of nanoparticles on the plain polystyrene particles, but allowed the positive surface of the aminated polystyrene particles to adsorb nanoparticles, if the new nonionic stabilizer was still adsorbed on the surface of the aminated polymer particles after acidic cleavage. Pluronic F108, a nonionic block copolymer containing blocks of poly(ethylene oxide) and poly(propylene oxide), was selected to replace the HPC.

After the acidic cleavage to release the amine group (in the form of $-\text{NH}_3^+$ in acidic aqueous medium), the polarity of the particles surface increased through losing the hydrophobic protecting groups. In this case, the acidic-treated particles could be easily

dispersed in an aqueous medium. The adsorbed F108 molecules might have partially or fully desorbed from the surface of the particles and diffused into the aqueous medium. If the F108 molecules were partially dissolved, both the electrostatic repulsion (due to the positive charges on the surface of the aminated polystyrene particles) and the remaining F108 molecules helped to stabilize the particles; if all the F108 molecules were desorbed, the stabilization of the aminated polystyrene particles was basically taken over by electrostatic repulsion. However, this speculation had not been tested through further experiments.

A simple test for observing the adsorption of gold nanoparticles on the plain polystyrene particles, with HPC or F108 as the stabilizer, was to observe a color change from white to a red tint in the sediment when a solution of gold nanoparticles was mixed with the plain polystyrene particles and then centrifuged. The F108 stabilized plain polystyrene particles resulting from above process were observed not to adsorb Au nanoparticles in an acidic medium, even when treated with concentrated HCl aqueous solution (note the distinctly white sediment and red supernatant in Figure 3.8a); however, HPC stabilized plain polystyrene particles would adsorb Au nanoparticles and become reddish colored in the acidic medium (note the distinctly red/pink sediment and clear supernatant in Figure 3.8b). The effect of the Pluronic as a stabilizing molecule was apparent by the ability to easily re-disperse the particles after removal of the HPC.

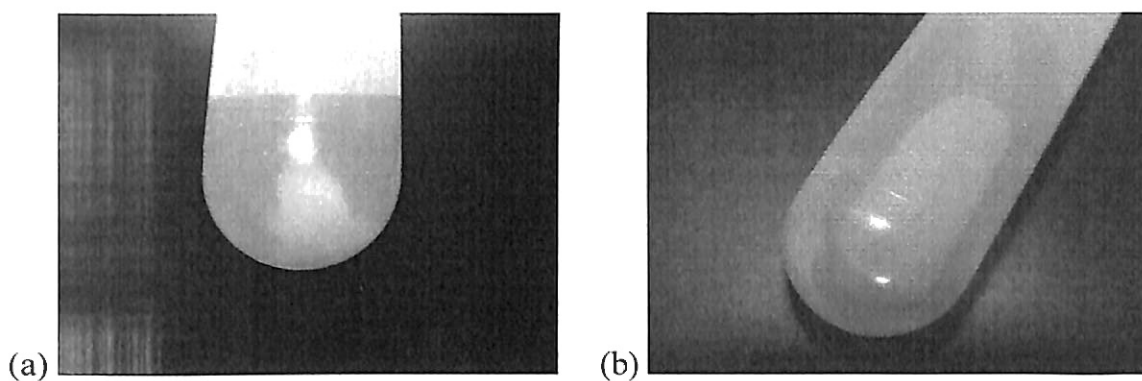


Figure 3.10 Adsorption test (a) white sediment after mixing Au nanoparticles with F108 stabilized plain polystyrene particles; (b) reddish sediment after mixing Au nanoparticles with HPC stabilized plain polystyrene particles

Scanning electron microscopy was used to qualitatively compare the surface coverage of the gold nanoparticles derived from sodium citrate and THPC reductions on aminated polystyrene particles. The sample SEM images in Figure 3.11 were simply deposited by placing a drop of the particle-containing suspension on a SEM stub, but the samples were not sputter coated with a gold film. The adsorption of sodium citrate reduced Au nanoparticles was relatively low resulting in sparse surface coverage. Thus, the significant surface charging on the sample and the poor imaging quality were shown in Figure 3.11a. In contrast, the coating of THPC reduced Au nanoparticles (1-3 nm) appeared dense, Figure 3.11 b, or at least continuous. In this case, the sample possessed enough conductivity to yield a good quality SEM image. Bright patches on the surface of these spheres may indicate some surface charging and a less than complete surface coverage.

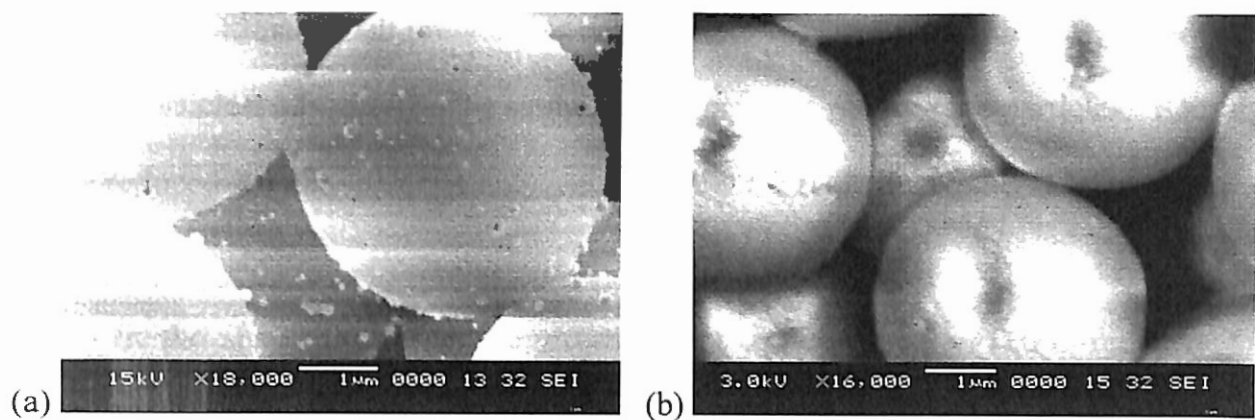


Figure 3.11 SEM images showing Au-polystyrene composite particles with (a) Au nanoparticles from sodium citrate reduction (b) Au nanoparticles from THPC reduction

In the test for the reversibility of the Au adsorption process, the Au nanoparticles were partially desorbed from the polymer particle surfaces if the pH of the aqueous medium had been increased, observed as the faded reddish tint of the sediment and the colored supernatant after centrifugation; after that, a reduction to the pH of the medium by addition of an HCl solution would restore complete adsorption of Au nanoparticles, observed as the darkened reddish tint of the sediment and the clear supernatant, which indicated the transfer of Au particles from the aqueous medium onto the surface of the polymer particles.

When the aminated polystyrene surface was coated with Au nanoparticles, instead of a shell structure, the adsorbed F108 molecules, if still available after the acidic de-protection step, were occupying a considerable percentage of the surface of the aminated polystyrene particles, so that both the steric hindrance and the electrostatic repulsion stabilized the polystyrene particles; if no F108 molecule was attached on the surface of the aminated polystyrene particles, the electrostatic repulsion alone stabilized the Au nanoparticle coated aminated polystyrene particles.

The gold nanoshell growth was only possible with the use of the THPC reduced Au nanoparticles, adsorbed on the surface of the aminated polystyrene particles. Sodium citrate reduced Au nanoparticles only grew bigger at the same reaction condition, without forming a nanoshell.

In the suspension state, the growth of the Au coating (by THPC reduced Au nanoparticles) on the surface of the aminated polystyrene particles reduced the stability of the composite particles, and tended to promote aggregation and precipitation. Thus, a cationic polyelectrolyte, polyethylenimine (PEI), was added to the suspension to assist the stabilization after the Au nanoshell growth, as shown in Figure 3.12.

The fact that the PEI helped to re-stabilize the aminated polystyrene particles after the Au nanoshell growth, as described in section 3.2.7, further suggests that a nanoshell-like structure formed.

If there were still Pluronic stabilizer F108 molecules attached on the polymer particles surface after the adsorption of Au nanoparticle, the formed Au nanoshell either displaced the Pluronic stabilizer or obscured its steric stabilizing effect. If the former were true, the gold nanoshell would possess a negative charge on the outer layer and the desorbed Pluronic would no longer associate with the polar surface to perform the stabilizing function, but would either be solubilized in the solvent or form small aggregates of the polymer chains.

As the Au nanoshell grew, the composite particles were carrying the positive charges on the underlying ionized amine groups, and the negative charges on the Au nanoshell structure, which was possibly with tens of nanometers thickness, depending on the concentration of the gold salt added in the first place. The stabilizer Pluronic F108

might or might not attached on the surface of the underlying polymer surface; if still attached, the effect of the F108 might be displaced or obscured by the Au shell as discussed above; the outer surface of the Au nanoshell was covered with stabilizing agents, which was only able to stabilize Au nanoparticles of size around 1-3 nm.

Hence, there were many interactions to consider for the emerging Au nanoshell composite structures. We suspect that, after a critical point, the repulsion, resulting from the positive-positive charges on the amine groups, and from the negative-negative charges on the Au nanoshells, and the steric hindrance (if still available), were not strong enough to counterbalance the electrostatic attractions between the positive and the negative charges, and the van der Waals force between the composite structures as well. As a result, the stabilizing effect was diminishing during the nanoshell growth.

On the other hand, the surface of underlying aminated polystyrene could be only weakly positive under the specific reaction condition, i.e., not sufficient electrostatic repulsion to impart colloidal stability for the whole composite particles.

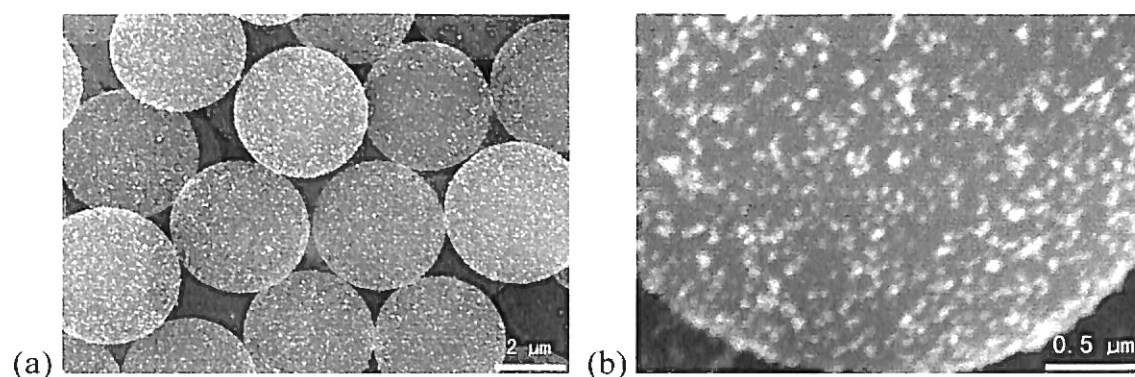


Figure 3.12 SEM images of Au nanoshell composite particles (a) 3.8 μm sized Au nanoshell composite particles (b) the surface of a Au nanoshell composite particle

Thereafter, the adsorption of positively charged PEI on the negatively charged Au

nanoshell was required to establish electrosteric stabilization.

The composite particles with Au nanoshell structure, grown from THPC reduced Au nanoparticles, Figure 3.11b, produce better SEM images without sputtering by comparison, as shown in Figure 3.12. Au nanoshell on the surface of polymer particles covers much larger area, and forms continuous conductive layer. Thus, most of the electrons are grounded without significant negative charge buildup on the particles surface so that clear SEM images could be taken. No image was shown for the non-growth of the Au nanoshell when sodium citrate reduced Au nanoparticles were the seeds.

The optical color change during Au seeds growth was observed to depend on the original size of the Au seeds (images not shown). Aminated polystyrene particles coated with THPC reduced Au seed (1-3 nm) became bluish-colored, indicating the nanoshell formation; while those polystyrene particles sparsely coated with sodium citrate reduced Au seed (~30 nm) became reddish-colored, which was possibly due to the size increase of the individual Au seeds, rather than a shell formation.

References

1. J. H. Braybrook and L. D. Hall, *Progress in Polymer Science*, **15**, 715-734 (1990).
2. V. L. Covolan, L. H. I. Mei and C. L. Rossi, *Polymers for Advanced Technologies*, **8**, 44-50 (1997).
3. A. Dokoutchaev, J. T. James, S. C. Koene, S. Pathak, G. K. S. Prakash and M. E. Thompson, *Chemistry of Materials*, **11**, 2389-2399 (1999).
4. D. G. Grier, *MRS Bulletin*, **23**, 21-21 (1998).
5. R. D. Averitt, D. Sarkar and N. J. Halas, *Physical Review Letters*, **78**, 4217-4220 (1997).
6. C. L. Haynes and R. P. Van Duyne, *Journal of Physical Chemistry B*, **105**, 5599-5611 (2001).
7. S. R. Sershen, S. L. Westcott, N. J. Halas and J. L. West, *Journal of Biomedical Materials Research*, **51**, 293-298 (2000).
8. G. Bosma, C. Pathmamanoharan, E. H. A. de Hoog, W. K. Kegel, A. van Blaaderen and H. N. W. Lekkerkerker, *Journal of Colloid and Interface Science*, **245**, 292-300 (2002).
9. A. Kondo and H. Fukuda, *Colloids and Surfaces a-Physicochemical and Engineering Aspects*, **153**, 435-438 (1999).
10. X. L. Xu, G. Friedman, K. D. Humfeld, S. A. Majetich and S. A. Asher, *Chemistry of Materials*, **14**, 1249-1256 (2002).
11. J. J. Storhoff and C. A. Mirkin, *Chemical Reviews*, **99**, 1849-1862 (1999).
12. S. L. Westcott, S. J. Oldenburg, T. R. Lee and N. J. Halas, *Langmuir*, **14**, 5396-5401 (1998).
13. T. Pham, J. Jackson, N. J. Halas and T. R. Lee, *Abstracts of Papers of the American Chemical Society*, **218**, U419-U419 (1999).
14. I. Miraballes-Martinez, A. Martin-Molina, F. Galisteo-Gonzalez and J. Forcada, *Journal of Polymer Science Part a-Polymer Chemistry*, **39**, 2929-2936 (2001).
15. I. Miraballes-Martinez and J. Forcada, *Journal of Polymer Science Part a-Polymer Chemistry*, **38**, 4230-4237 (2000).

16. S. Gibanel, V. Heroguez, Y. Gnanou, E. Aramendia, A. Bucsi and J. Forcada, *Polymers for Advanced Technologies*, **12**, 494-499 (2001).
17. A. Bucsi, J. Forcada, S. Gibanel, V. Heroguez, M. Fontanille and Y. Gnanou, *Macromolecules*, **31**, 2087-2097 (1998).
18. T. Delair, V. Marguet, C. Pichot and B. Mandrand, *Colloid and Polymer Science*, **272**, 962-970 (1994).
19. V. L. Covolan, S. D'Antone, G. Ruggeri and E. Chiellini, *Macromolecules*, **33**, 6685-6692 (2000).

Chapter 4

FABRICATION OF COLLOIDAL BUILDING BLOCKS

4.1 Introduction

In chapters two and three, synthesis of monodisperse spherical particles for the fabrication of colloidal building blocks was described. For clarity, colloidal building block (CBB) will be used to refer to an assembly of colloidal particles into a unit that is more than one particle in size. The colloidal building block moniker refers to the intended use of the CBB in the assembly of extended colloidal crystals. In this chapter, a process for the assembly of colloidal building blocks with desired 3D structures is presented. The process involves trapping spherical particles in a photoresist template, thermally fusing the particles into a cluster, and releasing them from the template. The process is a modification to the TASA developed by Xia, et al., described in chapter 1. The modified TASA process is described in the current chapter and special attention is given to the important steps necessary for the fabrication of the photoresist template and assembly of a fluidic cell.

The TASA process appears to be the most versatile technique available for designing non-spherical colloidal building blocks. However, other techniques for fabricating non-spherical particles bear mentioning, for example: ellipsoidal polymer beads can be formed by uni-axially stretching spherical beads²⁻⁴, ellipsoidal hematite

particles have been formed using a gel-sol process⁵, and peanut-shaped colloids have been formed through phase separation⁶⁻⁸. While the shapes formed by these techniques are certainly interesting, the techniques lack the degrees of freedom to truly design intricate CBB geometries and have no mechanism for altering local surface chemistry within the CBB.

In the TASA process, uniform aggregates with well-controlled sizes, shapes, and structures have been assembled with the use of a fluidic cell. The structure of the fluidic cell contains a top glass substrate with a hole for injecting the colloidal particles, a patterned bottom substrate, and a Mylar film with a thickness of tens of microns, which is sandwiched between the top and the bottom substrate and confines the dewetting liquid slug in the cell, Figure 4.1. A suspension of spherical particles is injected into the fluidic cell, which is inclined by a certain angle, and the fluid is allowed to de-wet the template as it flows through the cell. The trailing liquid/air interface causes a local increase in particle concentration near this meniscus and increases the diffusion rate of particles into the holes of the template in this region. The colloidal particles are subject to capillary force, buoyancy, gravity, and frequently electrostatic repulsion. The trapping of the colloidal particles is a collective result of all these interactions.

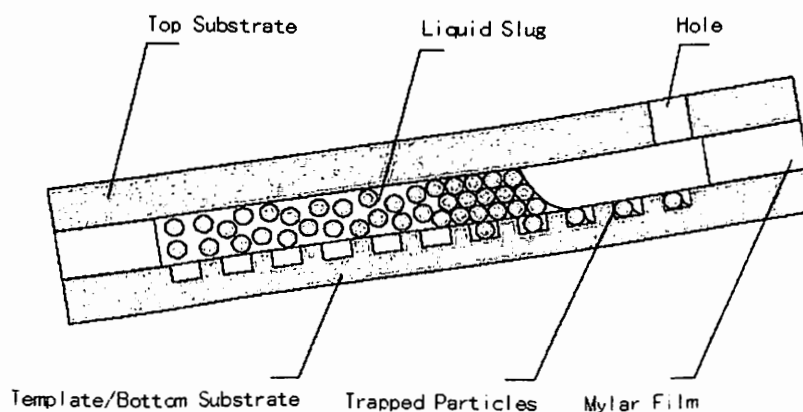


Figure 4.1 A dewetting fluidic cell for trapping spherical particles

Xia, et al. demonstrated a number of CBB geometries by the TASA method, Figure 1.5, using single holes to capture multiple particles. The capability of this method to trap a single particle precisely, into a cylindrical hole of an almost equivalent size on the template, has not been demonstrated, i.e., the size of the holes on the template in previous demonstrations was frequently 1.5 times that of the particles, or even larger, at least in one dimension. Although the particles are localized within the template holes, the position of the particles in these holes is less precise. The dewetting direction of the liquid slug was used, to some extent, to orient the trapped particles; in practice, it is extremely hard to control the direction and uniformity of the trailing edge of the liquid slug as it flows through the fluidic cell, so that it is very hard to precisely control the final position of the particles localized in the template holes. This drawback limits the capability of this TASA strategy to assemble complex 3D aggregates through precisely depositing spherical particles of different sizes into complex template through multiple dewetting processes in sequence.

The modification to the TASA strategy presented in this chapter explores the use of precision sequential particle trapping in a designed template to produce 3D CBB. To succeed in making the 3D CBB, sequential filling and draining of the fluidic cell to trap the particles, intermediate, second layer lithography to fabricate the template layers, and high precision alignment steps to construct the 3D template are required. While the ultimate goal of assembling a tetrahedral CBB was not accomplished in this work, the initial steps in the modified TASA process were developed. Possible procedures to assemble tetrahedral CBB in the future work using multi-layered templates in a modified TASA process are described in chapter 5.

The principle of photolithography is based on the radiation-induced chemical and physical alteration of highly specialized photosensitive polymeric films, called photoresists. Typically, a photomask is fabricated using a quartz or sodium lime glass plate, coated with an opaque material (usually chromium) bearing the design patterns. For a typical process, a photoresist is applied onto a substrate wafer, which is vacuum-mounted on a spinner, to form a thin uniform film through high-speed spinning. After baking to evaporate organic solvent and harden the resist film, selected areas of the photoresist are exposed using the photomask and an irradiation source. The exposed regions of the polymer exhibit a difference rate of removal in certain chemical reagents, resulting in the formation of a relief image of the mask, called development. For semiconductor processing, the pattern formed delineates the area for the subsequent modification of the underlying substrate in the unprotected regions. These steps are illustrated in the flow chart of Figure 4.2. Here, however, the relief mask is the template desired for the TASA process.

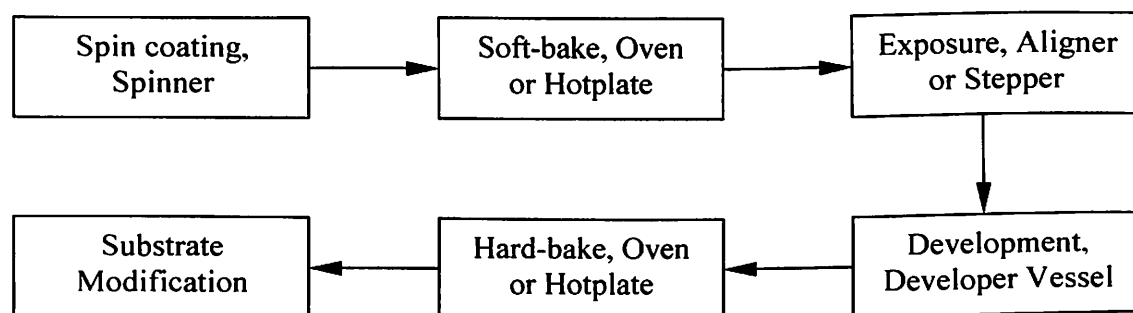


Figure 4.2 Illustration of a general photolithography process

Depending on the chemical nature of photoresists, either a positive or a negative relief image of the original mask emerges in the substrate after development as illustrated

in Figure 4.3. Resists that produce negative images undergo crosslinking upon irradiation, rendering them hard to dissolve in the developer solution, often an organic solvent. Positive resists experience molecular modification, after which acid functional groups are generated, which enhance the solubility of positive resists in basic developer solutions such that the exposed regions are removed at a faster rate than the unexposed ones. A negative resist is preferred in this work due to the consideration that a crosslinked polymer film from the negative resist is chemically much more stable than that from the positive resist. This is a desired property for the dewetting process where the film is exposed to an aqueous dispersion of polymer particles, and has to tolerate the variation of pH of the dispersion.

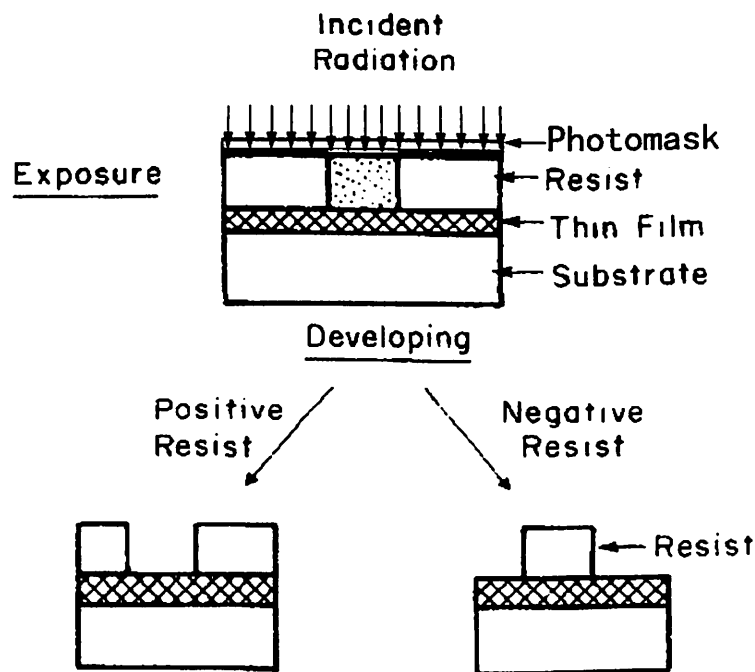


Figure 4.3 Principles of lithography illustrated for positive and negative resists

The photomask is itself made by a lithographic process. Although silver halide emulsions and iron oxide have been used in the past for mask making, today most high

quality glass masks are manufactured using chromium. The chromium can be deposited by sputtering, vacuum deposition, or CVD. The desired and computer-designed pattern data is first transferred to an automated laser or e-beam pattern generator. This pattern, in turn, is transferred into the resist layer overlying a thin film of chromium on the glass substrate. After the lithography is complete, the chromium is wet or dry etched to produce the mask pattern.

The photomask design and fabrication is a crucial step for the TASA process, not only because of the cost of making such a photomask, but also due to the fact that the relief structure on the template needs to be well planned to trap the particles into the desired 2D pattern. However, designing such a photomask is not as trivial as a simple geometric design. The final design should account for numerous, linked uncertainties in the photolithography process. In this work the particles are synthesized to a size that is compatible with the minimum feature sizes possible with the aligner. Thus the size of particles and the size of features in the mask design are intertwined. Additionally, the chemical and physical properties of the photoresist greatly influence the final geometric precision of the 3D relief structure; however, predicting the resolution of sharp edges in the photoresist is difficult at best and the possibility that features in the template may not be as crisp as designed must be considered when designing the mask. User technique in adjusting the aligners and executing the spinning and development processes are also factors along with the uniformity of photoresist removal rates and anisotropy. Given this litany of difficulties, a certain amount of trial and error iteration is necessary to produce the desired template and this implies some iterations of mask design.

Fortunately, the nature of the mask design allows for the production of an array of almost identical pattern sets in a single mask; the only difference among these pattern sets is their dimensions, which increased slightly one pattern set after the other. If the array of the dimensions was appropriately chosen, at least one patterns set would be suitable for the trapping of particles of specific sizes. In this way, many designs tested in parallel during a single run in the TASA fluidic cell.

4.2 Experimental

4.2.1 Materials

Three-inch diameter single-side polished and double-side polished silicon wafers were purchased from Waferworld, West Palm Beach, FL. Negative tone photoresist SU-8 2015 and SU-8 developer were purchase from Microchem, Newton, MA. Positive tone photoresist PR1-4000A and its developer RD6 were purchased from Futurrex, Franklin, NJ. Isopropanol (IPA) (270490-4L) was supplied by SigmaAldrich, Milwaukee, WI. Mylar films with thickness 0.0005", 0.001" and 0.002" were supplied by Fralock of Lockwood Industries, Canoga Park, CA. 3/16" clear Plexiglas plates were purchase from Lowe's.

4.2.2 Instrumentation

A programmable spinner, WS-400 Spin Processor, (Laurell Technologies Corporation, North Wales, PA) was used for the spin-coating process. An aligner, Kasper Wafer Alignment Systems Kasper 2001, (Kasper Instrument, Mountain View,

CA) was used for the exposure of the photoresist. A convective oven, Class 100 Clean Room Oven 3490M, (Barnstead International, Dubuque, Iowa) was used for pre-bake and post-bake processing. A plasma generator, PX-250, (March Plasma Systems, Concord, CA) was used to oxidize the surface of the photoresist template after development and baking. An optical microscope, Nikon Industrial Microscope Eclipse L150/L150A, (Nikon Instruments Inc. Melville, NY) was used to capture the images of assembled building blocks.

4.2.3 Photomask Fabrication

As mentioned earlier, the photomask design requires precise sizing and arrangement of the template holes and this was accomplished by a trial and error method utilizing an array of template designs. For monodisperse polystyrene particles of sizes approximately 4 μm and 6.5 μm , an example template structure is illustrated in Figure 4.7. Here, the larger particle in the central portion of the template is trapped in a first run in the TASA cell followed by trapping of the two smaller particles in a second run. The elevation of the three particles above the substrate was varied by design of the template as illustrated in Fig. 4.4b.

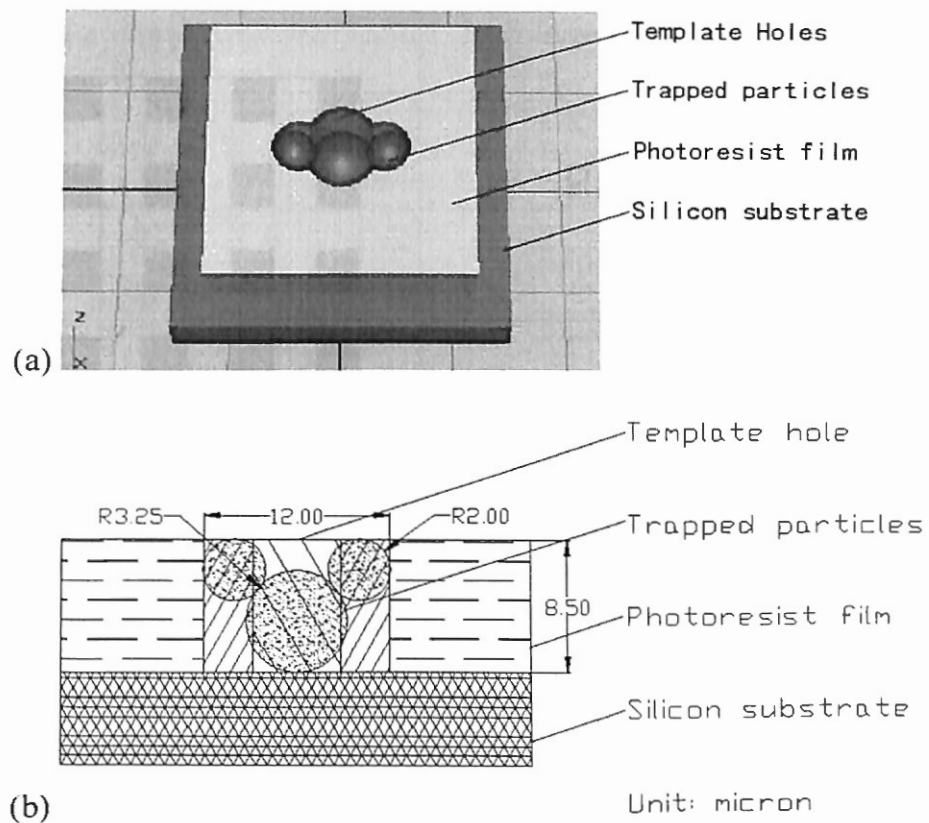


Figure 4.4 A relief photoresist structure trapping two $4\ \mu\text{m}$ polystyrene particles atop one $6.5\ \mu\text{m}$ polystyrene particles (a) perspective view (b) cross section view with dimensions

For trapping the particles effectively while precisely locating their positions within the holes, the size of the relief structures was designed slightly larger than actual size of the three-particle cluster illustrated in Fig 4.4. The extent to which the template size should be larger than particle size was determined experimentally by trial and error. The arrayed pattern sets on the photomask for the negative photoresist are illustrated in Figure 4.5.

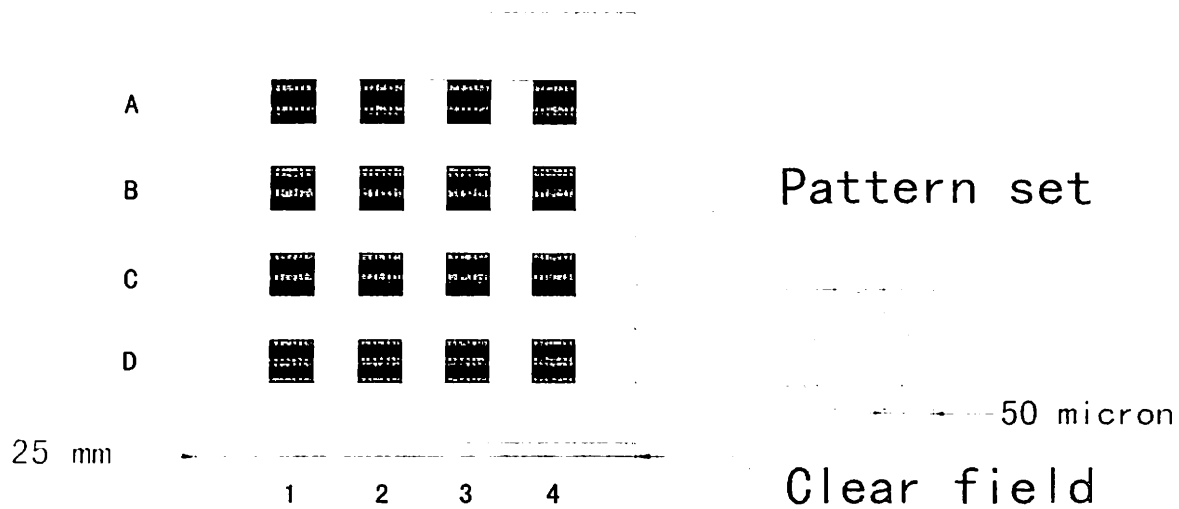


Figure 4.5 Layout of the array of the pattern sets on the photomask for the negative photoresist

The actual geometry of the patterns within each square of the array in Figure 4.5 are summarized as: in column 1 and column 2, each pattern is formed with one big circle at the center and two small circles symmetrically located at satellite positions, as shown in Figure 4.6; the three centers are collinear, the distance between the centers of the small circles is fixed at 8 μm ; the corresponding diameters referenced to the row and column markers in Figure 4.5 are listed in Table 4.1

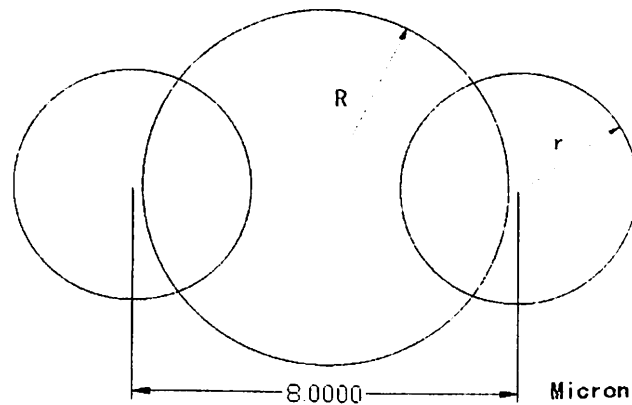


Figure 4.6 Shape of patterns in column 1 and column 2 on the mask design, consisting of 3 circles

Table 4.1 Dimensions of the patterns in column 1 and column 2 in the mask design (μm)

	A		B		C		D	
	R	r	R	r	R	r	R	r
1	3.8	2.45	3.9	2.55	3.95	2.65	4	2.75
2	3.5	2.05	3.55	2.15	3.6	2.25	3.7	2.35

In column 3 and column 4, each pattern is formed with one big ellipse at the center and two small circles symmetrically located at satellite positions, as shown in Figure 4.7. The three centers are collinear, the distance between the centers of the small circles is fixed at 8 μm; the corresponding diameters of the circles and the lengths of the axis of the ellipses are listed in Table 4.2

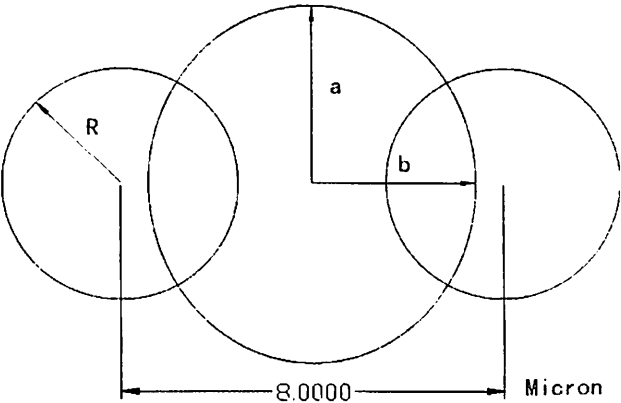


Figure 4.7 Shape of patterns in column 3 and column 4 on the mask design, consisting of two small circles and one big ellipse

Table 4.2 Dimensions of the patterns in column 3 and column 4 in the mask design (μm)

	A			B			C			D		
	R	a	b	R	a	b	R	a	b	R	a	b
3	2.45	3.8	3.43	2.55	3.9	3.48	2.65	3.95	3.52	2.75	4	3.56
4	2.05	3.5	3.3	2.15	3.55	3.32	2.25	3.6	3.34	2.35	3.7	3.37

The patterns were designed using AutoCAD 2002 software, in the DXF format. The photomask was fabricated through the Fasttrack program of Photosciences, Torrance, CA. A photomask with chromium on 4" X 4" X 0.09" Quartz glass (4090CRQZ) dark field was fabricated with an automatic laser pattern generator. Critical dimension for the features on the mask was set at 3 μm . Another photomask with a variety of patterns was also fabricated using the Fasttrack program of Photosciences, Torrance, CA. The second photomask was for the positive resist PR1-4000A.

4.2.4 Photolithography

The photolithography processes for making the template for the TASA were performed in the Class 1000 Ultrafast THz Optoelectronics Laboratory (UTOL) cleanroom in the ATRC basement. The oxygen plasma oxidation step was outside the Class 1000 environment. The typical processing steps used to fabricate both negative and positive photoresist relief structures are presented below. The aligner, (Kasper Wafer Alignment Systems Kasper 2001, Kasper Instrument, Mountain View, CA) used to fabricate the template is shown in Figure 4.8.



Figure 4.8 Kasper Wafer Alignment Systems, Kasper 2001

4.2.4.1 Negative photoresist processing

The chemical resistance and precision reproduction of features characteristic of the negative photoresists made these the favored material for the production of TASA templates. A 3" silicon wafer and negative tone photoresist SU-8 2015 was used. Initially, the wafer was concentrically vacuum-mounted on the spinner WS-400. Afterwards, approximately 3 mL of the very viscous negative photoresist was evenly dispensed onto the center of the wafer surface, with a disposable pipette. Air bubbles trapped within the dispensed photoresist, if any, were carefully extracted using a micropipette. The spinner was then programmed to ramp to 5500 rpm at an acceleration of 500 rpm/second and to continue spinning at 5500 rpm for another 29 seconds. The spin-coated wafer was then pre-baked for 1 minute on a contact hotplate at 65°C, followed by a soft-bake for 2 minutes on a contact hotplate at 95°C. Subsequently, the photomask was pressed in contact mode onto the resist film, which was then exposed to ultraviolet (UV) light from the mercury lamp for 25 seconds. The exposed resist was backside baked on a hotplate for 1 minute at 65°C, followed by a backside baking on a hotplate for 2 minutes at 95°C. An adequate amount of SU-8 developer was poured in a 4" petri dish. The post-baked wafer was immersed in the developer, with gentle agitation applied. After 3 minutes and 30 seconds, the wafer was removed from the developer and briefly rinsed with IPA and then dried with a stream of compressed air. At this point, the surface of the photoresist is hydrophobic. It was oxidized to improve wetting behavior using an oxygen plasma for 30 seconds with March Plasma Systems PX-250 under the following processing parameters: RF power 200 watt, base pressure 80 m τ and operating pressure 400 m τ .

4.2.4.2 Positive photoresist processing

To fabricate a template with a film thickness around 4 μm using the positive tone photoresist PR1-4000A, the following procedures were followed. Initially, a 3" wafer was concentrically vacuum-mounted on the spinner WS-400. Afterwards, approximately 3 mL of the positive photoresist was evenly dispensed onto the center of the wafer surface, with a disposable pipette. The spinner was then programmed to spin at 3000 rpm/second till a total time of 30 seconds was reached. The spin-coated wafer was then pre-baked for 10 minutes in the convective oven at 100°C. Subsequently, photomask was pressed in contact mode with the resist film, which was then exposed to UV light from the mercury lamp for 80 seconds to reach a total dose of 280 mJ/cm² for the 4 μm thick resist film. A post exposure bake for 3 minutes at 100°C in the convection oven was optional. Adequate amount of RD6 developer was poured in a 4' petri dish. The wafer was immersed in the developer, with gentle agitation applied. Visual inspection was crucial for determining the completion of the developing process. The development time for positive resist was not easily determined, due to the chemistry of the positive resist. After the development was deemed complete, the wafer was removed from the developer and briefly rinsed with deionized water and then dried with a stream of compressed air.

4.2.5 Modified TASA Method

4.2.5.1 Fabrication of Fluidic Cells

The structure of the fluidic cell used in this work is schematically illustrated in Figure 4.1, which was constructed by sandwiching a thin frame of Mylar film between

two substrates. A small hole of 1.5 mm in diameter was drilled on the top Plexiglas substrate prior to assembly. Before the assembly of the cell, the top 3" round Plexiglas substrate had been rinsed with ethanol and deionized (DI) water. The bottom substrate with the SU-8 2015 negative photoresist template film had been treated with the oxygen plasma (March Plasma Systems PX-250), as mentioned above, to make the surface hydrophilic. The square frame of Mylar film (0.002" thick) was cut with a razor blade and then rinsed with DI water. The cell was then assembled, with another 3" round Plexiglas substrate supporting the silicon wafer. A gentle stream of ethanol was injected into the cell to expel air, followed by a gentle stream of DI water to replace ethanol without introducing air bubbles. Next, a micropipette tip filled with DI water was connected to the hole on the top substrate. At this point the whole cell was clamped with binder clips to press the Plexiglas, Mylar, and wafer layers together.

4.2.5.2 Trapping of Spherical Colloids

After the fluidic cell had been assembled, a dispersion of monodisperse polystyrene microspheres with 6.4 μm mean diameter, which had been redispersed with SDS in water, was dripped into the micropipette tip. The polystyrene particles diffused into the cell gradually, due to the specific gravity of the polystyrene particles (1.05) and the number-concentration of the particles in the tip. Once the dispersion of colloids had filled the water-occupied space between the top and bottom substrates, the micropipette tip with excess liquid within was removed. The liquid slug of polystyrene dispersion confined between the substrates was then allowed to move slowly due to the water

evaporation and the flow of the water through the interfaces between the Mylar film and the substrates.

After the liquid slug had dewetted the surface of the bottom substrate and the remaining water evaporated, the 6.4 μm polystyrene particles were trapped in the template holes on the bottom substrate. At this point the *fluidic cell* was carefully disassembled. If the dewetting conditions (i.e., substrate speed) had been carefully controlled, the surface of the photoresist film was free from adsorbed polystyrene particles, except for those particles accumulated at the edge of the Mylar film frame. The accumulated polystyrene particle piles were removed using water-soaked cotton swabs. After the removal, the bottom substrate was put into an oven for 1 minute at 100°C to fix the 6.4 μm polystyrene particles within the template holes through viscoelastic deformation, as shown in Figure 4.11a, which was corresponding to the region set C-4. The polystyrene particles trapped and the template holes could not be fully visualized together due to the field depth of the optical Nikon Industrial Microscope Eclipse L150/L150A (Nikon Instruments Inc. Melville, NY). Quality of the trapping for the particles in the rest pattern sets was inferior to that in region C-4, as shown in 4.11b, where some template holes contained more than one polystyrene particle each due to the increased template geometry. This drastic change reflects the importance of the trial and error parallel-trapping method to identify the best design for the template holes.

To assemble building blocks as shown in Figure 4.4, a second similar step of dewetting was performed using the bottom template with trapped larger particles and a suspension of smaller monodisperse polystyrene particles. Although the template had been designed for 6.4 μm and 4 μm particles, the 4 μm particles did not work well with

the 6.4 μm particles and the template fabricated. Hence, a new batch of polystyrene particles of diameter around 3.7 μm was synthesized, by modifying the ratio of ethanol to 1-methoxy-2-propanol. The recipe was: 35 mL ethanol, 7.5 mL 1-methoxy-2-propanol as dispersion medium; 1 g HPC stabilizer (MW=60,000); 7.5 mL distilled styrene monomer with 0.5 g BPO initiator; reaction condition was the same as described in chapter 2. The resulting particles were washed with ethanol and redispersed in water by SDS. The optical image of the 3.7 μm polystyrene particles was shown in Figure 4.9.

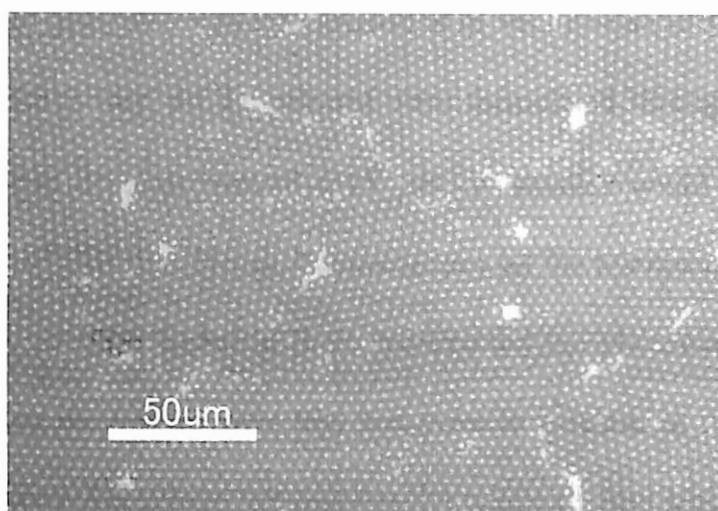


Figure 4.9 Monodisperse polystyrene microspheres synthesized for the second step trapping

These 3.7 μm particles were then trapped in the template holes, overlapping with the 6.4 μm particles trapped in the first step and form the building blocks.

4.3 Results and Discussion

4.3.1 Photomask Fabrication

Many considerations had been weighed in the design of the photomask; however, the patterns on the fabricated photomask might still not precisely represent the AutoCAD produced image. The laser pattern generator used at Photosciences, Torrance, CA carried a minimum pixel size of around $0.15\text{ }\mu\text{m}$ due to its laser beam resolution. The pattern on the photomask were generated through raster-scan or vector-scan of the laser beam on a photoresist film; either way, all the patterns were formulated through dots of $0.15\text{ }\mu\text{m}$ size or so such that features around $0.15\text{ }\mu\text{m}$ or smaller could not be accurately reproduced from the DXF file. Hence, Photosciences set the tolerance for this fabrication process at $\pm 0.35\text{ }\mu\text{m}$. This technical limit undermined the photomask quality to some extent, necessitating the use of some trial and error in fabricating the TASA template. The advantage of the laser pattern generator is the relatively low cost. An alternative to the laser pattern generation is to use more expensive e-beam lithography to fabricate the photomask, which ordinary delivers minimum pixel size around $0.02\text{ }\mu\text{m}$. At this point in this work it is unknown if this level of precision is necessary. Future attempts to refine the template design may require such cutting edge equipment.

4.3.2 Photolithography

Upright sidewalls of the template patterns were always preferred; however, without knowing the characteristics of the photoresist to be used, it would be dangerous to assume that upright sidewalls could be achieved. Under-exposure, over-exposure,

under-development and over-development of the photoresist all possibly result in angled sidewalls; isotropic etching, Figure 4.10, also leads to an exaggerated diameter of the upper part of the holes, especially in the case of a positive photoresist. Thus the decision on the hole sizes to be drawn with AutoCAD at design stage must tolerate these potential problems.

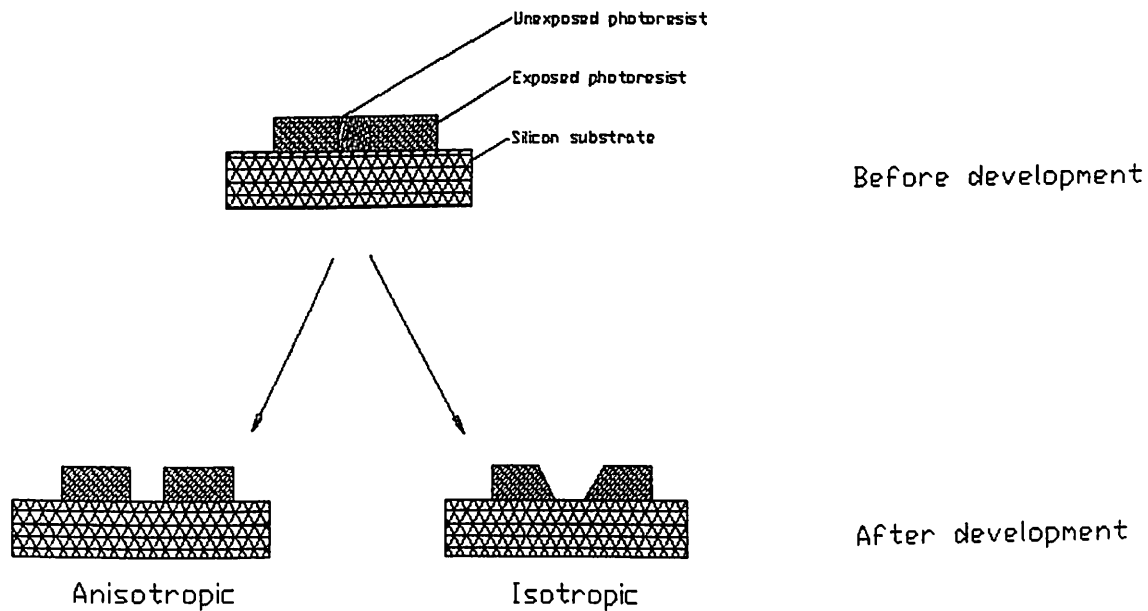


Figure 4.10 Schematic illustration of isotropic and anisotropic etching occurred during photoresist development

In addition, the diffraction of the UV exposure light was a constant issue. When the feature size was comparable to the wavelength of the UV light, diffraction became particularly problematic. In the photomask design, the intersection of two arcs, as shown in Figure 4.4 — Figure 4.7, produced features comparable to the wavelength of the UV light. The structure of those detailed features on the photomask could never be precisely transferred to the photoresist film due to this diffraction. Thus, the exposed structures were somewhat different from the photomask even before it was developed.

In the development stage, photoresist at sharp corners or fine features dissolved faster in the solvent. Hence, no template profile with sharp edges could be accurately reproduced after the development. This also made the patterns on the template different from what had been designed. The designed patterns were shown in Figure 4.6 and Figure 4.7.

After the plasma oxidation, the surface of the resist film became hydrophilic, which is a desired property for the following TASA process to be described in the next section.

The thickness of the resulting resist film was around 9.5 μm before oxygen plasma etching. When the final spin speed was changed to 5000 rpm but the other processing parameters remained the same, the resulting thickness of the photoresist film was around 12 μm ; at a spin speed of 6000 rpm, the resulting thickness of the photoresist was around 8 μm . An optical image of the fabricated template was shown in Figure 3.11 below. This particular template corresponds to pattern set D-4 from Table 4.2

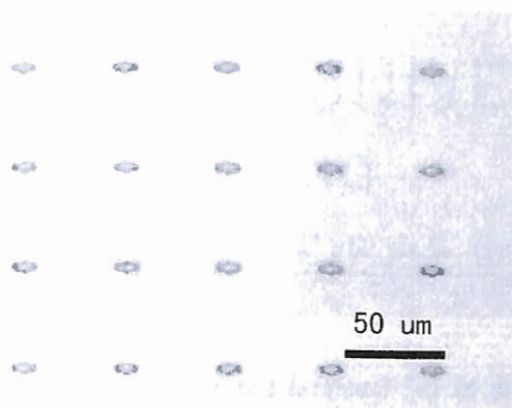


Figure 4.11 A template fabricated with the photomask and the negative photoresist

A template for trapping monodisperse 4.0 μm polystyrene particles is shown in Figure 4.12. Negative photoresist PR1-4000A was used for this fabrication.

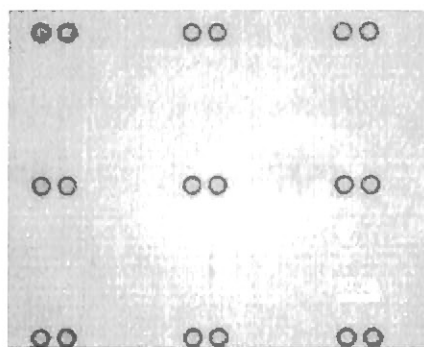


Figure 4.12 A positive template for trapping monodisperse 4.0 μm polystyrene particles

Despite the processing difficulties, usable photoresist templates were produced as evidenced by the successful trapping of particles, in Figure 4.13a and Figure 4.14. For future progress, however, a study of the relative effects of the template variations of particle trapping efficiency should be performed. For the purpose of this study, feasibility was the primary concern and optimization of the process variables was left as future work.

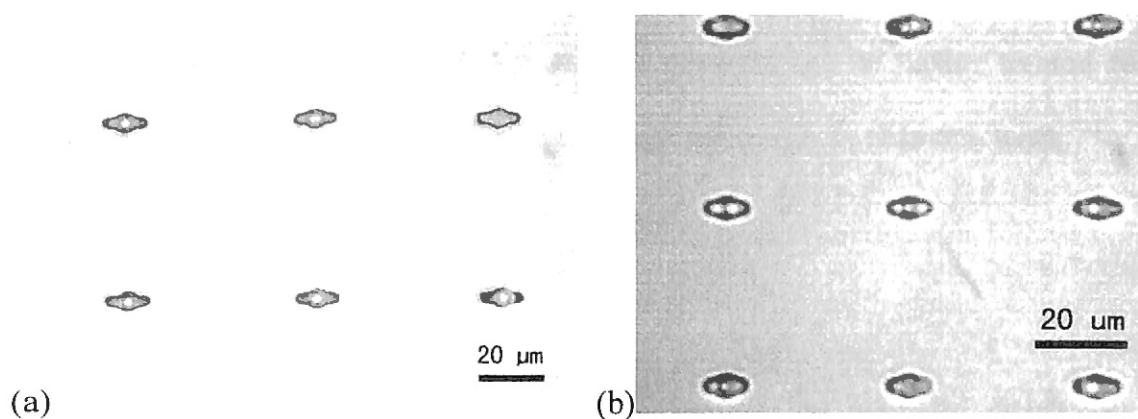


Figure 4.13 6.4 μm polystyrene microspheres trapped (a) at the center of the template holes in region C-4, (b) when the template holes (in region D-1) were with poor geometries; two particles were trapped in a single hole

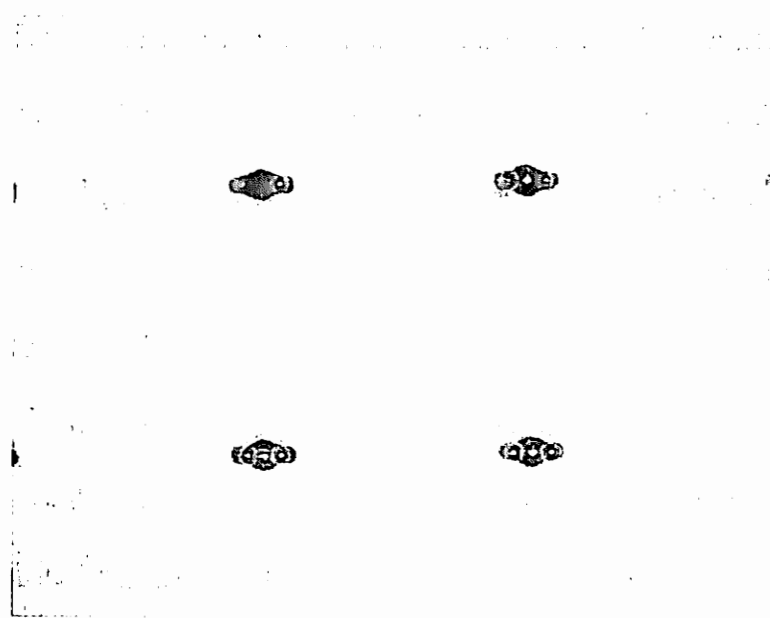


Figure 4.14 Triplet aggregates trapped in the template holes

After the trapping of the $3.7\ \mu\text{m}$ particles, shown as the smaller particles in Figure 4.14, these triplet structures could be fused together when subject to a temperature higher than the T_g of polystyrene. A sonication bath in DI water can be used to release the fused particles from the template holes; and the particles can be further treated for the self-assembly of colloidal crystal structures, though not covered yet in this work.

4.3.2 Modified TASA Method

The concentration of the colloidal particles in the aqueous dispersion was important to the successful trapping of the particles. The particles always had certain probability, albeit low, of simply falling into the template holes as a result of sedimentation. If a dilute dispersion had been used, there would be less than enough polystyrene particles confined in the fluidic cell such that the trailing-edge effect (i.e., locally increased particle concentration near the trailing meniscus) would have been

insignificant leading to only a few particles being trapped. When particle concentration becomes high enough, the majority of the template holes were observed to be completely occupied by colloidal particles, even before the rear edge of the liquid slug had passed through these regions. On the other extreme, if too many particles had been transferred into the fluidic cell, the diffusion of particles away from the high concentration region near the trailing meniscus would have been insufficient to prevent the formation of a deposited particle bed (i.e., a filter cake) and further trapping of particles was inhibited.

The template hole sizes in Younan Xia's work were generally 1.5-2 times of that of particles to be trapped. While this difference facilitated a *high trapping efficiency*, it compromised the precise positioning of the particles in the template. This work needs precision location of the particles within the template holes; however, trapping efficiency decreased when the holes were closer in size to the particles. When hole sizes were between 1-1.5 times of that of the particles, it was found more difficult to trap the particles, Figure 4.15. When the two sizes were almost identical, it was *extremely* difficult to achieve a high trapping ratio.

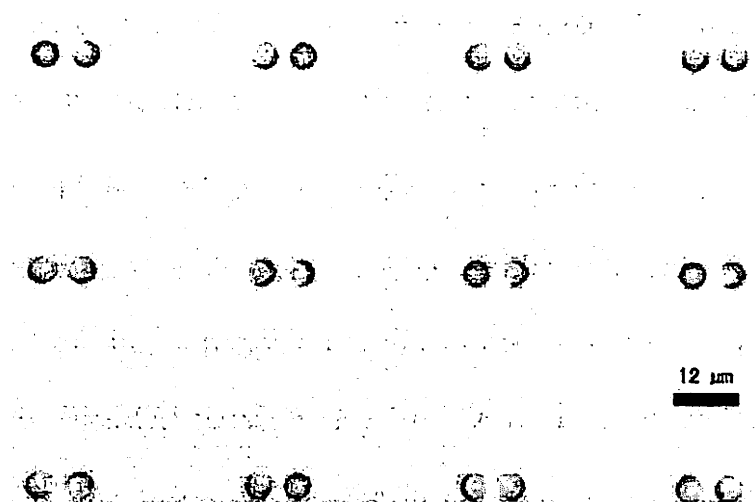


Figure 4.15 particles of 4 μm diameter trapped in 4.7 μm holes; with some vacant holes

Due to the optical effects, these particles were shown as dark rings surrounding bright central dots. Only monodisperse polystyrene particles were investigated in the modified two-step TASA process so far. The plain polystyrene particles will be replaced with amine-functionalized polystyrene particles in future work.

The surface charge of the photoresist template in an aqueous medium need to be controlled, after the oxygen plasma oxidation step. The same-signed surface charge on the surface of the polymer particles was preferred, which would produce a repulsive interaction between the colloidal particles and the surface of the template, ensuring that no particle would adsorbed to the templates. In that case, the colloidal particles could be to some degree levitated from the template surface by a certain distance when the colloidal dispersion was flowing through the fluidic cell. Therefore, the capillary force created by the liquid meniscus was able to push the colloidal particles across the surface of the bottom substrate unless they were physically trapped by the template holes.

The use of dispersant SDS also aided to the free flowing of the polymer particles in the fluidic cell. The SDS molecules tended to accumulate and self-arrange at the interfaces; in the case of TASA process, theses SDS molecules would be covering the template/water and the particle/water interfaces, which would bear negative charges due to the ionized hydrophilic head group $-\text{SO}_4^-$. This electrostatic repulsion also helped to keep polymer particles from sticking to the surface of the template.

In the case of simple templates such as cylindrical holes, the structures of the trapped aggregates were determined by the ratio between the dimensions of the template and the diameter of the spherical colloids; in the case of multiple step trapping with

complex templates, the outcome was determined by the sequence of trapping, the size of the particles used in each step of trapping, and the dimension of the photoresist template.

The speed of water dewetting generally had no effect on the final results, unless the speed was too fast and the concentration of the particles was high. If so, the inertia of the polymer particles and the resistance resulting from the collisions among the particles might overcome the pulling effect from the rear edge of the receding meniscus. In that case, the particles might separate from the aqueous medium and remain on the surface of the template.

Air bubbles in the liquid slug during dewetting, if exist, would change the flow direction of the aqueous medium and hinder the particles from moving freely; it also altered the shape of the trailing meniscus. Thus, any air bubble should have been carefully removed before polymer particles were transferred into the fluidic cell.

The Mylar film thickness did not have a substantial effect on the trapping process, unless the produced gap between the top and bottom substrates was so small that the polymer particles were not allowed to flow without too many collisions.

The direction of the trailing meniscus was not a controllable factor to induce preferred orientation of the trapped particles. The particles transferred into the fluidic cell generally were not evenly distributed; as the meniscus receded, the particles accumulated so that the corresponding resistances generated at different locations varied, which would translate into the unpredictable change of the direction of the trailing meniscus, hence a uncontrollable change of the orientation of the trapped particles.

Only the template fabrication step was performed in the Class 1000 cleanroom. The fluidic cell assembly and the particles dewetting processes were open to airborne

contaminants, which could lead to less than perfect trapping results. A cleaner environment would help to simplify the processing conditions, achieve higher trapping ratio and more reproducible results.

The success of this two-step TASA process was based on the success of both steps. In the second step, the two polystyrene particles at satellite positions were fairly easily trapped because the dimensions of the particles were noticeably smaller than the geometric confinement; in the first step, however, the trapping ratio was not high enough, due to the requirement on precise positioning, which in turn demanded closely comparable particle size and template geometry. To get better trapping ratio in the first step of trapping, the mechanism of the particles trapping process needs to be improved to facilitate the demand. Other potential means include directing the motion of the particles into the template holes by using external fields, such as an electric field, a magnetic field, or a combination of both, concerted with the dewetting mechanism of the TASA process.

After the formation of the complex building blocks and thermal annealing, the photoresist pattern may be removed by dissolving with a solvent, if possible. It is an optional step before a sonication bath is used to release the particles from the substrate. There was no good solvent for the SU-8 2015 negative photoresist. However, if a positive resist or a dissolvable negative photoresist, other than SU-8 2015, was used, this dissolution step would help to release the fabricated CBB.

The amine-functionalized polystyrene particles have not been test-trapped in the TASA process yet. However, the surface chemistry of the functionalized polystyrene particles can be tuned to facilitate the success of such kind of TASA process. After all, it is theoretically similar, if not identical, to trap either functionalized or plain polystyrene

particles, as long as the additional surface functionality doesn't induce electrostatic attractions between the particles and the template surface, which will also be investigated in the future work.

In conclusion, this chapter demonstrates: 1) the successful fabrication of the designed CBB with the desired 3D structure from monodisperse polystyrene dispersions, through a two-step dewetting process using a micro-structured template; 2) the sizes of the monodisperse polystyrene particles have been tailored to fit the geometric confinement of the template holes;

References

1. J. J. Storhoff and C. A. Mirkin, *Chemical Reviews*, **99**, 1849-1862 (1999).
2. M. Nagy and A. Keller, *Polymer Communications*, **30**, 130-132 (1989).
3. P. Jiang, J. F. Bertone and V. L. Colvin, *Science*, **291**, 453-457 (2001).
4. Y. Lu, Y. Yin and Y. Xia, *Advanced Materials*, **13**, 415-420 (2001).
5. Y. Lu, Y. Yin and Y. Xia, *Advanced Materials*, **13**, 271-274 (2001).
6. H. R. Sheu, M. S. Elaasser and J. W. Vanderhoff, *Abstracts of Papers of the American Chemical Society*, **196**, 252-Pmse (1988).
7. A. T. Skjeltorp, J. Ugelstad and T. Ellingsen, *Journal of Colloid and Interface Science*, **113**, 577-582 (1986).
8. M. Okubo, T. Yamashita, T. Suzuki and T. Shimizu, *Colloid and Polymer Science*, **275**, 288-292 (1997).
9. O. D. Velev, K. Furusawa and K. Nagayama, *Langmuir*, **12**, 2374-2384 (1996).
10. W. T. S. Huck, J. Tien and G. M. Whitesides, *Journal of the American Chemical Society*, **120**, 8267-8268 (1998).
11. O. D. Velev, A. M. Lenhoff and E. W. Kaler, *Science*, **287**, 2240-2243 (2000).
12. A. vanBlaaderen, R. Ruel and P. Wiltzius, *Nature*, **385**, 321-324 (1997).
13. K. H. Lin, J. C. Crocker, V. Prasad, A. Schofield, D. A. Weitz, T. C. Lubensky and A. G. Yodh, *Physical Review Letters*, **85**, 1770-1773 (2000).
14. G. A. Ozin and S. M. Yang, *Advanced Functional Materials*, **11**, 95-104 (2001).
15. S. M. Yang and G. A. Ozin, *Chemical Communications*, 2507-2508 (2000).
16. J. Tien, A. Terfort and G. M. Whitesides, *Langmuir*, **13**, 5349-5355 (1997).
17. J. Aizenberg, P. V. Braun and P. Wiltzius, *Physical Review Letters*, **84**, 2997-3000 (2000).
18. K. M. Chen, X. P. Jiang, L. C. Kimerling and P. T. Hammond, *Langmuir*, **16**, 7825-7834 (2000).

19. Y. Yin, Y. Lu, B. Gates and Y. Xia, *Journal of the American Chemical Society*, **123**, 8718-8729 (2001).

Chapter 5

CONCLUSIONS AND RECOMMENDATIONS

5.1 Conclusions

The overall objective of this work was to explore a modified template assisted self-assembly process to fabricate novel colloidal building blocks for the eventual directed self-assembly of colloidal crystals. This thesis highlights significant accomplishments that support this overall objective; however, the assembly of the colloidal building blocks into a colloidal crystal has yet to be demonstrated. Nonetheless, the accomplishments in this thesis are plentiful and are listed in this conclusion chapter along with recommendations for future investigation. For example, monodisperse plain polystyrene microspheres with controlled sizes were synthesized through dispersion polymerization. A method to add chemical functionality to a thin surface layer without altering the particle size was successfully executed. Selective adsorption of gold nanoparticles onto functionalized polystyrene particles was demonstrated. Finally, micron-sized complex building blocks were fabricated through a modified TASA method using the pre-synthesized polystyrene particles. The key points of these accomplishments are summarized below in the order they were discussed in the thesis.

1. The dispersion polymerization of styrene monomer in the presence of a nonionic stabilizer dissolved in an organic medium was studied. The effects of the

reaction temperature, the solvency of the dispersion medium, and the concentrations of the monomer, the initiator and the stabilizer on the size and the monodispersity of the synthesized polymer particles were discussed. By controlling these process variables, monodisperse particles in the size range of 3.5 μm to 6.4 μm were synthesized to serve as the spherical particles for assembly of complex building blocks. Some refinement of particle size was performed by centrifugation to remove small and large outliers.

2. A two-step polymerization method was used to synthesize monodisperse, amine-functionalized polystyrene particle in the desired size range of 3.5 μm to 4.0 μm .

3. The surface chemistry of polystyrene particles synthesized through the two-step process could be modified by simple changes in the comonomer composition in the second step. This facile process allows for the creation of functionalized particles while maintaining the ease of dispersion polymerization to create monodisperse particles under similar reaction conditions for the plain polystyrene particles.

4. The surface chemistries of the plain polystyrene particles and the amine-functionalized polystyrene particles were shown to selectively adsorb gold nanoparticles within a specific pH range; i.e., the plain particles do not adsorb Au nanoparticles, but the aminated polystyrene particles adsorbed significant amounts of Au nanoparticles. For both types of particles, a nonionic stabilizer, Pluronic F108, was substituted for the synthesis stabilizer, HPC, to eliminate the tendency of the HPC to adsorb Au nanoparticles.

5. Gold nanoshell structures were synthesized by the adsorption of negatively charged Au nanoparticles on the surface of the positively charged polymer particles in the first step, and then by growth of an Au shell by the reduction of gold salt in a basic

aqueous medium in the second step. The *gold nanoshell* structures were intended for use in the complex colloidal building blocks to serve as substrates for attaching thiolized complimentary oligonucleotides strands to direct self-assembly into a colloidal crystal.

6. Complex colloidal building blocks consisting of a large central particle and two satellite particles were assembled using a modified template assisted self-assembly (TASA) process. A photomask was designed based on the sizes of the monodisperse polymer particles and the structure of the complex building blocks to be assembled. Arrayed sets of patterns on the single photomask were generated to test the candidate patterns with progressively increasing dimensions in a parallel manner. This arrayed variation in geometry was used to account for the numerous process variations that led to non-ideal pattern transfer from the photomask to the photoresist, and to target the optimal geometry for the selected polystyrene particles in the TASA process.

7. The photoresist template for the TASA process was fabricated through photolithography. Both positive and negative photoresists were used to generate a variety of patterns for the particle trapping. A template generated using the negative photoresist was used for the TASA process.

8. A two-step TASA process was performed to selectively and sequentially trap different-sized polystyrene particles into the template holes. The assembly of the complex building blocks with the desired geometries had been accomplished. The factors leading to a successful TASA process were discussed. The best set of patterns among the designed for the assembly of the complex building block structure was identified.

The accomplishments listed here are important steps in fabricating a new type of colloidal building block for colloidal crystals. The interdependent nature of the photomask design, photolithography, TASA process, and particle size necessitated the need to produce monodisperse particles of a size compatible with available photolithography equipment. Thus, the dispersion polymerization process developed facilitated the easy control of particle size by controlling the concentration of solvents and reactants in the synthesis. The substitution of a less toxic solvent in this process was a valuable step to improving the user friendliness of the process. The absence of localized, controlled variations in surface chemistry in colloidal building blocks for self-assembly limits the types of crystal structures that may be assembled to those reliant solely on geometry. The amine modification of the polystyrene surface combined with the stabilizer replacement demonstrated both the feasibility of synthesizing monodisperse particles of the desired size with altered surface chemistry and the ability to selectively adsorb Au nanoparticles on these particles. Thus, while these modified particles were not used in the TASA process, the important foundational steps have been accomplished.

5.2 Recommendations and Future Work

The work discussed in this thesis lays the groundwork for the next step in development: to assemble colloidal building blocks by TASA containing both plain and aminated polystyrene particles in a single cluster. Thus, when these building blocks are released from the template into suspension, we hypothesize that the locally varied surface chemistry may allow for selective adsorption of Au nanoparticles and/or functionalized

oligonucleotides to direct colloidal crystallization. The current work was exploratory in nature, however, several aspects can be improved and processes optimized.

5.2.1 Process Optimization

1. Fractional centrifugation is effective in removing large and small outlier particles; however, a large fraction of desirable particles are lost due to the inefficiency of this process. More efficient and sophisticated separation techniques, such as Field Flow Fractionation, may be used to harvest monodisperse particles.

2. The growth of Au nanoshells by seeding the growth on adsorbed nanoparticles appeared to yield continuous nanoshells. The reaction variables (i.e., salt concentration, pH, temperature) may be explored to discover the most suitable conditions for higher Au coverage on the polymer particle substrates.

3. The production of the photoresist template is highly susceptible to user technique and experience. A study of process variations and the relative sensitivity of features in the produced template would be useful to guide better photomask design and improve particle trapping efficiency in the TASA process.

4. As an alternative to photolithography, a photomask fabricated through e-beam lithography would improve geometric control.

5. Alternative positive or negative photoresists should be evaluated to identify the one for the best performance of the fabricated photoresist template.

6. The processing conditions could be simplified and the results of particles trapping could be improved if the assembly of the fluidic cell and the dewetting processes had been performed in the cleanroom.

5.2.2 Recommended Future Work

1. The desire for selective directional bonding in colloidal crystals implies that the amine-functionalized polystyrene particles are to be used in the second step of the TASA process: Au nanoshells are to be selectively coated on to the two amine-functionalized polystyrene particles of the already-assembled complex building structures. Suitable conditions for assembly of the composite building blocks as well as solution conditions (e.g., pH, temperature, salt concentrations) for selective adsorption of Au nanoparticles onto the aminated parts of the colloidal building blocks need to be identified.

2. Thiolized complementary oligonucleotides strands attached to the gold-coated portions of two batches of colloidal building blocks may be used to direct the assembly of such particles into a desired crystal structure. The solution conditions amenable to oligonucleotides attachment to the particles and for **complexation** of complimentary strands need to be identified and the crystallization of an ensemble of these colloidal building blocks needs to be attempted.

3. A modification to add 3D structure of the complex building blocks, e.g. a tetrahedral structure, is more advantageous than the current CBB design. A tetrahedral CBB may lead to a diamond-like crystal lattice, as illustrated in Figure 5.1. However, it requires a more sophisticated **photolithography** capability and a multi-step dewetting process.

The diamond-like photonic lattice (Figure. 5.1d) is to be assembled from the **building blocks** with a tetrahedral structure, which is made of four satellite particles strategically registered on the **surface of the** center particle (Figure. 5.1a). In the structure of a tetrahedral building block, the central polystyrene particle **acts as the linkage** among

satellite particles, which are coated with complementary thiolized oligonucleotides. A more complex template strategy is to be used to facilitate the fabrication of the tetrahedral building block structures, as the steps of which are illustrated in Figure 5.2. Figure 5.2a shows two of the satellite particles that have been trapped in a first iteration of the TASA process and the photoresist template has been prepared for the second stage of trapping by dissolving the elliptical hole in the center. Next, a second layer of photoresist is patterned and used for capture of the central polystyrene particle and remaining satellite particles (similar to the process illustrated in this thesis in Chapter 4) in Figure 5.2b. Finally, the captured particles are fused thermally and released from the template by dissolving the photoresist and sonication.

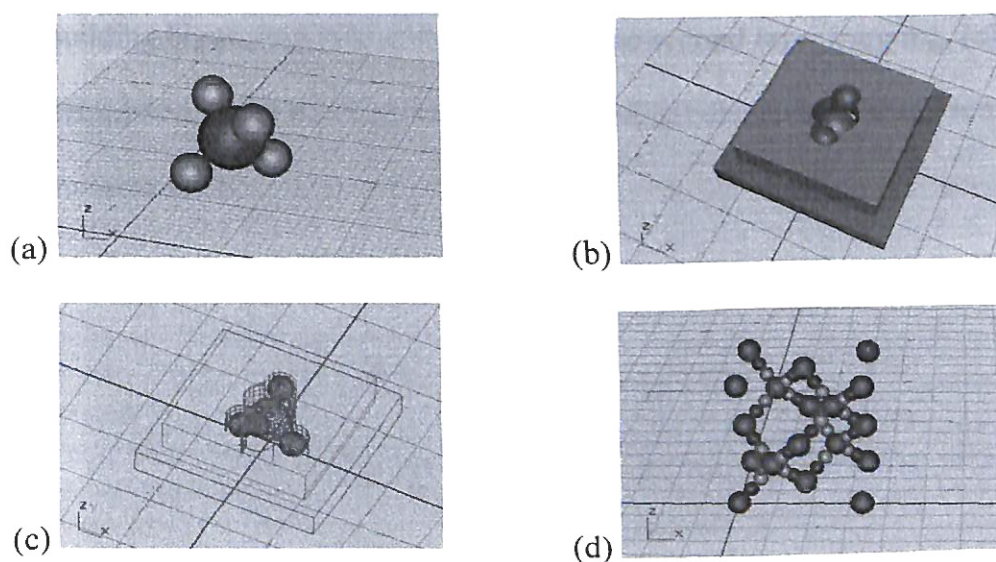


Figure 5.1 (a) A tetrahedral building block (to be assembled) without the template; (b) a tetrahedral building block structure trapped in the template (solid); (c) a tetrahedral building block structure trapped in the template (transparent); (d) a diamond-like lattice to be assembled from the tetrahedral building blocks

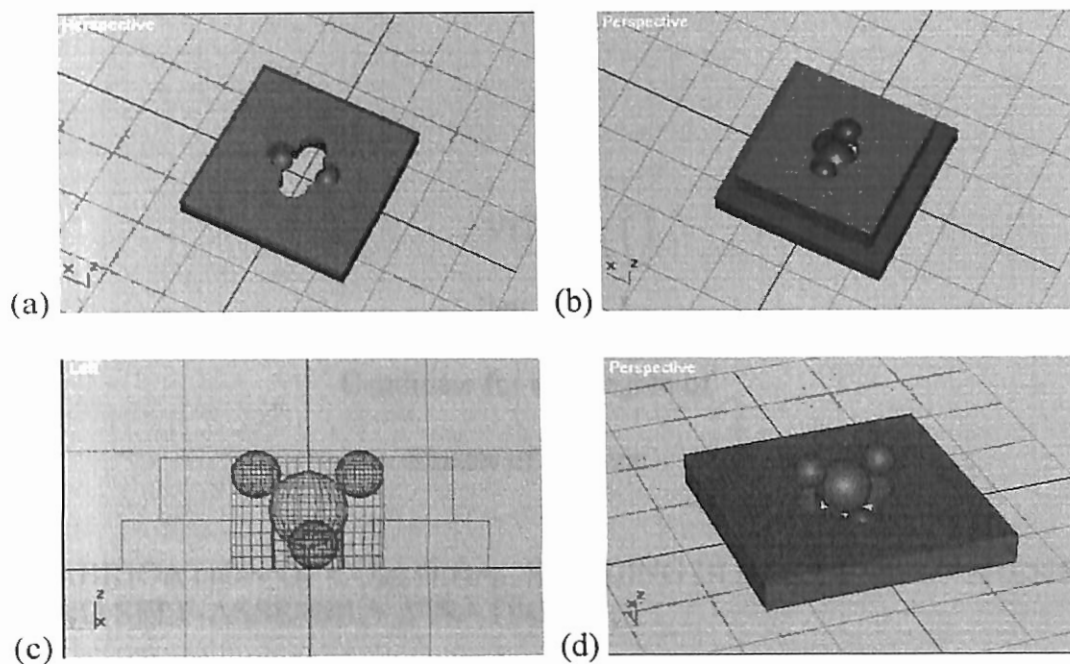


Figure 5.2 The illustration of a possible template strategy for assembling the tetrahedral shaped colloidal building blocks (a) the particles trapped in the first layer, (b) the tetrahedral building block structure assembled after the second layer trapping, (c) a side view of the template and the building block assembled, (d) dissolving the top template to release the building block

VITA ①

Jian Xu

Candidate for the Degree of

Master of Science

Thesis: FABRICATION OF COLLOIDAL BUILDING BLOCKS BY SYNTHESIS
AND SELF-ASSEMBLY STRATEGY

Major Field: Chemical Engineering

Biographical:

Personal Data: Born in Zhenjiang, Jiangsu Province, P. R. China, on February 10, 1976, the son of Xu, Jinlin and Hu, Ping

Education: Graduated from Zhenjiang No. 1 High School in June 1994; received Bachelor of Engineering degree in Chemical Engineering from Central South University, Changsha, Hunan Province, P. R. China. Completed the requirements for the degree of Master of Science degree with a Major in Chemical Engineering at Oklahoma State University in December, 2004

Experience: Employed by Gold East Paper (Jiangsu) Co., Ltd., Jiangsu Province, P. R. China as an engineer in 1998; employed as an engineer in SAE Magnetics (H.K.) Ltd., a wholly owned TDK subsidiary in 1999; employed by Oklahoma State University, School of Chemical Engineering as a graduate research assistant in 2001 to present